Journal of Computational Physics **148,** 467–496 (1999)
Article ID jcph.1998.6126, available online at http://www.idealibrary.com on IDEAL®

Numerical Solution of the Incompressible Navier–Stokes Equations with Coriolis Forces Based on the Discretization of the Total Time Derivative

Ramon Codina

Escola Tècnica Superior d'Enginyers de Camins, Canals i Ports, Universitat Politècnica de Catalunya, Jordi Girona 1–3, Edifici C1, 08034 Barcelona, Spain
E-mail: codina@cimne.upc.es

Received September 8, 1998

In this paper we present a numerical formulation to solve the incompressible Navier–Stokes equations written in a rotating frame of reference. The method is based on a finite difference discretization in time and a finite element discretization in space. When the viscosity is very small, numerical oscillations may appear due both to the high Reynolds number and to the presence of the Coriolis forces. To overcome these oscillations, a special discretization in time is proposed. The idea is to discretize the total time derivative in an inertial basis rather than only the partial time derivative in the rotating reference system. After this is done, a further high-order approximation is introduced, leading to a problem posed in the rotating frame of reference and in spatial coordinates. In contrast with the straightforward discretization of the original equations, some additional terms appear that enhance the stability of the numerical scheme. In the absence of Coriolis forces, the method is a generalization of the characteristic Galerkin technique for convection-dominated flows.

Key Words: incompressible flows; Coriolis forces; method of characteristics; inertial bases; stabilized finite element methods.

1. INTRODUCTION

The objective of this paper is to present a numerical formulation to solve the incompressible Navier–Stokes equations written in a rotating frame of reference. These equations are

$$\frac{\partial \boldsymbol{u}}{\partial t} + \boldsymbol{u} \cdot \nabla \boldsymbol{u} + 2\boldsymbol{\omega} \times \boldsymbol{u} - \nu \Delta \boldsymbol{u} + \nabla p + \boldsymbol{\omega} \times (\boldsymbol{\omega} \times \boldsymbol{r}) - \boldsymbol{f} = \boldsymbol{0}, \tag{1a}$$

$$\nabla \cdot \boldsymbol{u} = 0, \tag{1b}$$

0021-9991/99 $30.00

where $\boldsymbol{u}$ is the velocity field, p is the pressure divided by the (constant) density (i.e., the kinematic pressure), $\boldsymbol{f}$ is the vector of body forces, and ν is the kinematic viscosity of the fluid. The constant vector $\boldsymbol{\omega}$ is the velocity of rotation of the frame of reference and therefore $2\,\boldsymbol{\omega} \times \boldsymbol{u}$ and $\boldsymbol{\omega} \times (\boldsymbol{\omega} \times \boldsymbol{r})$ are the Coriolis and centrifugal forces, respectively. Equations (1) must be supplied with initial and boundary conditions that shall be introduced when necessary. The computational domain where the problem is to be solved is denoted by Ω and the time interval by $[0, T]$. The vector of position in this domain is denoted by $\boldsymbol{r} = (x_1, x_2, x_3)$. Here and below, a Cartesian coordinate system is assumed, with basis $\{\boldsymbol{e}_1, \boldsymbol{e}_2, \boldsymbol{e}_3\}$ in the three-dimensional case considered throughout.

There are several numerical difficulties associated with system (1). In the next two sections we shall address the problems found when the viscosity ν is very small and, hence, viscous forces are small compared either to the inertial forces or to the Coriolis forces. The dimensionless numbers used to quantify these effects are the Reynolds number Re and the Ekman number Ek, defined as

$$\mathrm{Re} := \frac{UL}{\nu}, \quad \mathrm{Ek} := \frac{\nu}{\omega L^2}, \tag{2}$$

where U is a characteristic velocity, L is a characteristic length, and $\omega = |\boldsymbol{\omega}|$. The numerical problems encountered when Re is high are well known. However, less attention has been paid to the problems arising when Ek is small, that is, when Coriolis forces dominate viscous forces. We treat this point in Section 3, where we present a method based on the same ideas as the characteristic Galerkin method described in Section 2 for convection dominated flows.

The basic idea of the numerical scheme proposed here is to write the conservation equations in an inertial frame of reference and discretizing the total time derivative using finite differences, instead of only the partial time derivative. In fact, this is the basic idea of the characteristic Galerkin method [1–3], although, to our knowledge, it has not been applied to the Navier–Stokes equations with Coriolis forces. The original characteristic Galerkin method is precisely the subject of the following section. We present here a particular version of this technique that generalizes some previous schemes [4] and shows its connection with other methods currently used for convection dominated flows [5–7] (see [8] for a comparison between all these methods).

The Coriolis and centrifugal forces of the Navier–Stokes equations arise because the velocity is expressed in a basis that varies in time. The discretization of the total time derivative involves therefore two different bases in a typical single step finite difference discretization. Both these bases must be expressed initially in terms of an inertial basis. In Section 3 we show how one of the rotating bases can be expressed in terms of the other, thus leading to a problem for the components of the momentum expressed in the latter. Since the starting point is writing the equations in an inertial reference system, we shall refer to this approach as the *inertial Galerkin method*.

It has to be stressed that the previous ideas are independent of the time discretization technique employed and, in fact, their motivation is based on the stability problems found *in space* when standard discretization techniques are used (centered finite differences or Galerkin finite element or spectral methods). However, the analysis presented here will be based on a particular time discretization, namely, the generalized trapezoidal rule, even though the possibility of using other time integration schemes is completely open.

In Section 4 some aspects related to the finite element method as a particular space discretization technique are described briefly. Finally, some numerical experiments are presented in the last section of the paper to show the effectiveness of the proposed scheme.

Let us introduce some notation now. Let $0 = t_0 < t_1 < \cdots < t_N = T$ be a partition of the time interval $[0, T]$. For simplicity of notation, we take the time step size $k := t_n - t_{n-1}$ constant, $n = 1, 2, \ldots, N$. For a generic function φ of the position $\boldsymbol{x}$ and the time t we use the abbreviation φ^n for $\varphi(\boldsymbol{x}, t_n)$ or for the approximation to it arising from a problem discretized in time. Also, for a number $\beta \in [0, 1]$ we define $\varphi^{n+\beta} := \beta\varphi^{n+1} + (1-\beta)\varphi^n$. The partial derivative with respect to the ith coordinate x_i is denoted either by $\partial\varphi/\partial x_i$ or simply by $\partial_i\varphi$, if there is no possibility of confusion. The Einstein convention is employed for repeated indices.

2. CHARACTERISTIC GALERKIN METHOD FOR THE INCOMPRESSIBLE NAVIER–STOKES EQUATIONS

2.1. *Description of the Method*

For the purposes of this section it is enough to consider now system (1) with $\boldsymbol{\omega} = \mathbf{0}$, that is,

$$\frac{\partial \boldsymbol{u}}{\partial t} + \boldsymbol{u} \cdot \nabla \boldsymbol{u} - \nu \Delta \boldsymbol{u} + \nabla p - \boldsymbol{f} = \mathbf{0}, \tag{3a}$$

$$\nabla \cdot \boldsymbol{u} = 0. \tag{3b}$$

Let us denote by $\boldsymbol{X}(\bar{\boldsymbol{x}}, \bar{t}; t)$ the trajectory of the particle that at time $t = \bar{t}$ is located at the spatial point $\bar{\boldsymbol{x}}$, so that $\boldsymbol{X}(\bar{\boldsymbol{x}}, \bar{t}; \bar{t}) = \bar{\boldsymbol{x}}$. This trajectory will be the solution of the problem

$$\frac{\mathrm{d}}{\mathrm{d}t} X_i(t) = u_i(\boldsymbol{X}(t), t), \tag{4a}$$

$$X_i(\bar{t}) = \bar{x}_i \tag{4b}$$

for $i = 1, 2, 3$. In the short-hand notation $\boldsymbol{X}(t)$ it is understood that $\boldsymbol{X}$ depends also on $\bar{t}$ and $\bar{\boldsymbol{x}}$, through the initial condition (4b).

The conservation of momentum and mass for a particle of incompressible fluid as it moves along its trajectory may be then written as

$$\frac{\mathrm{d}}{\mathrm{d}t}\boldsymbol{u}(\boldsymbol{X}(t), t) - \nu \Delta \boldsymbol{u}(\boldsymbol{X}(t), t) + \nabla p(\boldsymbol{X}(t), t) - \boldsymbol{f}(\boldsymbol{X}(t), t) = \mathbf{0}, \tag{5a}$$

$$\nabla \cdot \boldsymbol{u}(\boldsymbol{X}(t), t) = 0. \tag{5b}$$

Since

$$\frac{\mathrm{d}}{\mathrm{d}t}\boldsymbol{u}(\boldsymbol{X}(t), t)|_{t=\bar{t}} = \left(\frac{\partial \boldsymbol{u}}{\partial t} + \boldsymbol{u} \cdot \nabla \boldsymbol{u}\right)\Big|_{\boldsymbol{x}=\bar{\boldsymbol{x}}, t=\bar{t}} \tag{6}$$

Eqs. (5) for $t = \bar{t}$ are precisely the Navier–Stokes equations (3) at the spatial point $\boldsymbol{x} = \bar{\boldsymbol{x}}$ and at time $t = \bar{t}$. If there is no ambiguity, we shall use $\boldsymbol{x}$ instead of $\bar{\boldsymbol{x}}$, to emphasize that this position is arbitrary.

The idea now is to discretize the derivative $\mathrm{d}/\mathrm{d}t$ in Eq. (5a) using a finite difference scheme, that is, to discretize the total derivative in Eq. (3a) along the characteristics.

If we employ a single step finite difference discretization, the highest time accuracy that we can obtain is second order. In order to be as accurate as possible in the *first* (spatial) argument of the velocity and the pressure, problem (5) has to be discretized up to second order. Observe that the discretization in time in Eq. (5a) involves both the first and the second arguments of the velocity and the pressure, since we want to move along the characteristics. Once the second-order time discretization is done, different schemes can be obtained by approximating the *second* (temporal) argument of the velocity and the pressure, yielding discrete schemes with a lower temporal accuracy but potentially second-order accurate in space. Of course, our reference at the moment of considering the formal accuracy must be problem (5), and not problem (3), although both of them are completely equivalent at the continuous level. Obviously, time integration schemes of order higher than 2 can be used as well.

Suppose now that we have the solution at time t_n and we want to compute it at time t_{n+1}. Let $\bar{t}$ be a certain time in $[t_n, t_{n+1}]$ and define

$$\mathcal{S} := -\nu\Delta\boldsymbol{u} + \nabla p \tag{7}$$

as the Stokes contribution to the momentum equation. The discretization of problem (5) that we consider is based on the generalized trapezoidal rule (also called θ-method), which leads to

$$\frac{1}{k}[\boldsymbol{u}(\boldsymbol{X}(t_{n+1}), t_{n+1}) - \boldsymbol{u}(\boldsymbol{X}(t_n), t_n)] + \theta\mathcal{S}(\boldsymbol{X}(t_{n+1}), t_{n+1}) + (1-\theta)\mathcal{S}(\boldsymbol{X}(t_n), t_n)$$
$$- \theta\boldsymbol{f}(\boldsymbol{X}(t_{n+1}), t_{n+1}) - (1-\theta)\boldsymbol{f}(\boldsymbol{X}(t_n), t_n) = \boldsymbol{0}, \tag{8a}$$

$$\nabla\cdot\boldsymbol{u}(\boldsymbol{X}(\bar{t}), \bar{t}) = 0, \tag{8b}$$

where $\theta \in [0, 1]$. For the reasons explained above, we must take $\theta = 1/2$, since this is the only value of θ that yields second-order accuracy (Crank–Nicolson scheme).

It is observed from Eq. (8b) that the incompressibility restriction has been applied at the reference time $\bar{t}$, although this will be irrelevant for the final time discrete scheme, as we shall see.

The important point now is that we shall derive an explicit expression for the terms $\boldsymbol{u}(\boldsymbol{X}(t_{n+1}), t_{n+1})$ and $\boldsymbol{u}(\boldsymbol{X}(t_n), t_n)$, as well as for $\varphi(\boldsymbol{X}(t_{n+1}), t_{n+1})$ and $\varphi(\boldsymbol{X}(t_n), t_n)$ for a given function φ. This will allow us to obtain a semi-discrete system of equations, where all the terms will be evaluated at the same point of the same spatial domain. The parameter that we have still free is the reference time $\bar{t}$, which is associated with the reference coordinate system. Within the time step $[t_n, t_{n+1}]$ we shall take this time as $\bar{t} = t_n + \gamma k$, with γ arbitrary. Two particular cases of interest are $\gamma = 1/2$ and $\gamma = 1$, that is, $\bar{t} = t_n + k/2$ and $\bar{t} = t_{n+1}$. The former yields the classical Crank–Nicolson discretization of problem (3), whereas the later introduces some additional terms than enhance the stability of the numerical scheme. From the geometrical standpoint, if $\bar{t} = t_n + k/2$ Eq. (8a) (with $\theta = 1/2$) may be viewed as centered discretization along the characteristics. On the other hand, for $\bar{t} = t_{n+1}$ we move backwards. This is relative to the particle we follow although in both cases the discretization is formally of second order.

As has already been mentioned in the Introduction, even though our starting point is the generalized trapezoidal rule, the ideas introduced in what follows can also be applied

to any finite difference time discretization of the continuous equations. The only term the discretization of which will be dictated by the use of Eqs. (5) instead of Eqs. (3) is the convective one.

2.2. *Discretization along the Characteristics*

Let $\varphi(\boldsymbol{x}, t)$ be a generic function. The goal is to obtain a second- and a third-order approximation in time to $\varphi(\boldsymbol{X}(t_{n+1}), t_{n+1})$ and $\varphi(\boldsymbol{X}(t_n), t_n)$. For a same order of approximation, *we shall use explicit approximations*, instead of implicit ones. Thus, other schemes, apart from the one derived below, exist with the same properties of accuracy.

Let us first note that from Eqs. (4)

$$\begin{aligned}\boldsymbol{X}(t_{n+1}) &= \boldsymbol{X}(t_n + \gamma k) + (1-\gamma)k\,\boldsymbol{u}(\boldsymbol{X}(t_n + \gamma k), t_n) + O(k^2)\\ &= \boldsymbol{x} + (1-\gamma)k\,\boldsymbol{u}^n + O(k^2), \qquad (9a)\\ \boldsymbol{X}(t_n) &= \boldsymbol{X}(t_n + \gamma k) - \gamma k\,\boldsymbol{u}(\boldsymbol{X}(t_n + \gamma k), t_n) + O(k^2)\\ &= \boldsymbol{x} - \gamma k\,\boldsymbol{u}^n + O(k^2). \qquad (9b)\end{aligned}$$

Therefore, we may approximate

$$\begin{aligned}\varphi(\boldsymbol{X}(t_{n+1}), t_{n+1}) &= \varphi\big(\boldsymbol{x} + (1-\gamma)k\,\boldsymbol{u}^n + O(k^2), t_{n+1}\big)\\ &= \varphi^{n+1} + (1-\gamma)k\,\boldsymbol{u}^n \cdot \nabla\varphi^n + O(k^2), \qquad (10a)\end{aligned}$$

where we have made use of the fact that $\varphi^{n+1} = \varphi^n + O(k)$, an approximation frequently used hereafter. Similarly,

$$\varphi(\boldsymbol{X}(t_n), t_n) = \varphi^n - \gamma k\,\boldsymbol{u}^n \cdot \nabla\varphi^n + O(k^2). \qquad (10b)$$

Using Eqs. (10) taking the velocity $\boldsymbol{u}$ as the function φ, we can obtain a third-order approximation of the trajectory $\boldsymbol{X}$ solution of problem (4) as

$$\begin{aligned}\boldsymbol{X}(t_{n+1}) &= \boldsymbol{X}(t_n + \gamma k) + (1-\gamma)\frac{k}{2}[\boldsymbol{u}(\boldsymbol{X}(t_n + \gamma k), t_n + \gamma k) + \boldsymbol{u}(\boldsymbol{X}(t_{n+1}), t_{n+1})] + O(k^3)\\ &= \boldsymbol{x} + (1-\gamma)\frac{k}{2}[(1-\gamma)\boldsymbol{u}^n + \gamma\boldsymbol{u}^{n+1} + \boldsymbol{u}^{n+1} + (1-\gamma)k\,\boldsymbol{u}^n \cdot \nabla\boldsymbol{u}^n] + O(k^3)\\ &= \boldsymbol{x} + (1-\gamma)\frac{k}{2}[(1-\gamma)\boldsymbol{u}^n + (1+\gamma)\boldsymbol{u}^{n+1}] + (1-\gamma)^2\frac{k^2}{2}\boldsymbol{u}^n \cdot \nabla\boldsymbol{u}^n + O(k^3)\end{aligned} \qquad (11a)$$

and, similarly,

$$\boldsymbol{X}(t_n) = \boldsymbol{x} - \gamma\frac{k}{2}[(2-\gamma)\boldsymbol{u}^n + \gamma\boldsymbol{u}^{n+1}] + \gamma^2\frac{k^2}{2}\boldsymbol{u}^n \cdot \nabla\boldsymbol{u}^n + O(k^3). \qquad (11b)$$

Using Eqs. (11) we obtain the desired approximations to the function φ using again a Taylor expansion. This approximation is

$$\begin{aligned}\varphi(\boldsymbol{X}(t_{n+1}), t_{n+1}) = \varphi^{n+1} &+ (1-\gamma)\frac{k}{2}\big[(1-\gamma)u_i^n + (1+\gamma)u_i^{n+1}\big]\frac{\partial\varphi^{n+1}}{\partial x_i}\\ &+ (1-\gamma)^2\frac{k^2}{2}u_j^n\frac{\partial}{\partial x_j}\left(u_i^n\frac{\partial\varphi^n}{\partial x_i}\right) + O(k^3), \qquad (12a)\end{aligned}$$

and, in a similar way,

$$\varphi(\boldsymbol{X}(t_n),t_n)=\varphi^n-\gamma\frac{k}{2}\left[(2-\gamma)u_i^n+\gamma u_i^{n+1}\right]\frac{\partial\varphi^n}{\partial x_i}+\gamma^2\frac{k^2}{2}u_j^n\frac{\partial}{\partial x_j}\left(u_i^n\frac{\partial\varphi^n}{\partial x_i}\right)+O(k^3). \tag{12b}$$

These, together with Eqs. (10), are the expressions we were looking for. They represent approximations to the function φ along the trajectory of the particles (i.e., the characteristics of the total derivative operator) at the beginning and the end of the time interval $[t_n, t_{n+1}]$ under consideration.

2.3. *Semidiscrete Problem*

We shall apply Eqs. (10) and (12) now to obtain a second-orde approximation to the semidiscrete problem (8). From Eqs. (12) taking φ as the ith component of the velocity $\boldsymbol{u}$, we obtain

$$\begin{aligned}
&u_i(\boldsymbol{X}(t_{n+1}),t_{n+1})-u_i(\boldsymbol{X}(t_n),t_n)\\
&\quad=u_i^{n+1}-u_i^n+(1-\gamma)\frac{k}{2}\left[(1-\gamma)u_j^n+(1+\gamma)u_j^{n+1}\right]\partial_j u_i^{n+1}\\
&\qquad+\gamma\frac{k}{2}\left[(2-\gamma)u_j^n+\gamma u_j^{n+1}\right]\partial_j u_i^n+(1-2\gamma)\frac{k^2}{2}u_l^n\partial_l\left(u_j^n\partial_j u_i^n\right)+O(k^3)\\
&\quad=u_i^{n+1}-u_i^n+\frac{k}{2}\left[u_j^{n+\gamma}+u_j^{n+1-\gamma}\right]\partial_j u_i^{n+1-\gamma}\\
&\qquad+(1-2\gamma)\frac{k^2}{2}u_l^n\partial_l\left(u_j^n\partial_j u_i^n\right)+O(k^3),
\end{aligned} \tag{13}$$

where we have made use of

$$(1-\gamma)u_j^{n+1}\partial_j u_i^{n+1}+\gamma u_j^n\partial_j u_i^n=u_j^{n+1-\gamma}\partial_j u_i^{n+1-\gamma}+O(k^2). \tag{14}$$

This in turn is a consequence of the fact that for a given bilinear functional g,

$$g(\varphi^{n+\beta},\varphi^{n+\beta})=\beta g(\varphi^{n+1},\varphi^{n+1})+(1-\beta)g(\varphi^n,\varphi^n)+O(k^2). \tag{15}$$

Also, using the identity

$$\frac{1}{2}[\varphi^{n+\gamma}+\varphi^{n+1-\gamma}]=\varphi^{n+1/2}, \tag{16}$$

Eq. (13) may be written in vector form as

$$\begin{aligned}
&\boldsymbol{u}(\boldsymbol{X}(t_{n+1}),t_{n+1})-\boldsymbol{u}(\boldsymbol{X}(t_n),t_n)\\
&\quad=\boldsymbol{u}^{n+1}-\boldsymbol{u}^n+k\boldsymbol{u}^{n+1/2}\cdot\nabla\boldsymbol{u}^{n+1-\gamma}+(1-2\gamma)\frac{k^2}{2}\boldsymbol{u}^n\cdot\nabla(\boldsymbol{u}^n\cdot\nabla\boldsymbol{u}^n)+O(k^3).
\end{aligned} \tag{17}$$

From Eqs. (10) it is easy to see that

$$\frac{1}{2}[\varphi(\boldsymbol{X}(t_{n+1}),t_{n+1})+\varphi(\boldsymbol{X}(t_n),t_n)]=\varphi^{n+1/2}+(1-2\gamma)\frac{k}{2}\boldsymbol{u}^n\cdot\nabla\varphi^n+O(k^2). \tag{18}$$

Using Eqs. (17) and (18) in system (8) (with $\theta = 1/2$) we finally get the semidiscrete problem

$$\begin{aligned} &\frac{1}{k}[\boldsymbol{u}^{n+1} - \boldsymbol{u}^n] + \boldsymbol{u}^{n+1/2} \cdot \nabla \boldsymbol{u}^{n+1-\gamma} - \nu \Delta \boldsymbol{u}^{n+1/2} + \nabla p^{n+1/2} - \boldsymbol{f}^{n+1/2} \\ &\quad - (2\gamma - 1)\frac{k}{2}\boldsymbol{u}^n \cdot \nabla[\boldsymbol{u}^n \cdot \nabla \boldsymbol{u}^n - \nu \Delta \boldsymbol{u}^n + \nabla p^n - \boldsymbol{f}^n] = \boldsymbol{0}, \\ &\qquad\qquad\qquad\qquad\qquad\qquad\qquad\qquad \nabla \cdot \boldsymbol{u}^{n+1} = 0. \end{aligned} \tag{19}$$

The second equation in (19) is a second-order approximation of the incompressibility constraint imposed at $\bar{t} = t_n + \gamma k$ (see Eq. (8b)), since

$$\nabla \cdot \boldsymbol{u}(\boldsymbol{x}, t_n + \gamma k) = \gamma \nabla \cdot \boldsymbol{u}^{n+1} + (1 - \gamma)\nabla \cdot \boldsymbol{u}^n + O(k^2), \tag{20}$$

and assuming the initial condition to be divergence-free, the second equation in (19) is enough to ensure that $\boldsymbol{u}(\boldsymbol{x}, t_n + \gamma k)$ is also divergence-free up to second order.

It is observed from Eq. (19) that for $\gamma = 1/2$ we obtain the classical Crank–Nicolson approximation of the original problem (3), even though Eqs. (19) have been obtained from the discretization of problem (5). *A posteriori* we may, however, interpret them as the time discretization of problem (3) plus the introduction of the term

$$-(2\gamma - 1)\frac{k}{2}\boldsymbol{u}^n \cdot \nabla[\boldsymbol{u}^n \cdot \nabla \boldsymbol{u}^n - \nu \Delta \boldsymbol{u}^n + \nabla p^n - \boldsymbol{f}^n]. \tag{21}$$

Following this way, Eqs. (19) are only a first-order approximation to problem (3), whereas we have derived them as a (formally) second-order approximation to problem (5) and taking the reference coordinate system at time $\bar{t} = t_n + \gamma k$.

From problem (19) we can obtain simplified versions of first-order accuracy in time by replacing quantities at intermediate times between t_n and t_{n+1} either by values at t_n or t_{n+1} (explicit or implicit versions, respectively). Observe that this only involves an approximation in time, not in space. Neglecting the terms affected by the time step size in Eqs. (19) would imply also an approximation in space, since they come from an approximation of the characteristics $\boldsymbol{X}(t)$. Observe also that precisely the first term within the brackets in Eq. (21) is the one that will be responsible for the numerical stability of the scheme. For $\gamma > 1/2$, it provides a dissipation term that for divergence-free velocities $\boldsymbol{u}^n$ will be streamline oriented, the numerical viscosity being of magnitude

$$\nu_{\mathrm{sl}} = (2\gamma - 1)\frac{k}{2}|\boldsymbol{u}^n|^2. \tag{22}$$

This term arises also in other numerical techniques in similar forms using very different arguments, such as in the so-called SUPG and Taylor–Galerkin methods (see, e.g., Refs. [5, 7]).

The characteristic Galerkin method in its original form [1, 2] was designed as a crude first-order approximation in time (backward Euler scheme) and taking $\gamma = 1$ with our notation. It also has the drawback of having to integrate the trajectories at each time step and interpolating the value $\varphi(\boldsymbol{X}(t_n), t_n)$ within the element to which the point $\boldsymbol{X}(t_n)$ belongs. The idea of approximating the characteristics by using a Taylor expansion was introduced in Refs. [3, 4]. We have presented here a new and more general derivation particularized to

the incompressible Navier–Stokes equations. The ideas behind it will serve us also in the derivation of the numerical technique presented in the next section.

3. INERTIAL GALERKIN METHOD FOR THE INCOMPRESSIBLE NAVIER–STOKES EQUATIONS WITH CORIOLIS FORCES

3.1. *Introduction*

Another source of difficulties in the numerical solution of problem (1) when ν is very small arises because of the Coriolis force $2\boldsymbol{\omega}\times\boldsymbol{u}$. The reason for these oscillations is in essence the same as for the numerical problems encountered when there is a dominant convective term; it is impossible to have control over any of them. To see this, we will obtain now a stability estimate for $\boldsymbol{u}$ using a classical argument. For that, we consider the simple backward Euler time approximation of Eq. (1),

$$\frac{1}{k}(\boldsymbol{u}^{n+1}-\boldsymbol{u}^{n})+\boldsymbol{u}^{n+1}\cdot\nabla\boldsymbol{u}^{n+1}+2\boldsymbol{\omega}\times\boldsymbol{u}^{n+1}-\nu\Delta\boldsymbol{u}^{n+1}+\nabla p^{n+1}=\boldsymbol{f}_c^{n+1}, \tag{23}$$

where $\boldsymbol{f}_c=\boldsymbol{f}-\boldsymbol{\omega}\times(\boldsymbol{\omega}\times\boldsymbol{r})$ and we have assumed $\boldsymbol{f}$ continuous in time. Equation (23) must be supplied with the incompressibility constraint $\nabla\cdot\boldsymbol{u}^{n+1}=0$. Let us denote by $(\cdot,\cdot)$ the L^2 product in the domain Ω and by $|\cdot|$ the associated norm. To simplify the exposition, we take the homogeneous Dirichlet boundary condition $\boldsymbol{u}=\boldsymbol{0}$ on the whole boundary $\partial\Omega$. Multiplying Eq. (23) by $\boldsymbol{u}^{n+1}$, integrating over Ω, and using the facts that $\boldsymbol{u}^{n+1}$ is divergence-free and $(2a,a-b)=|a|^2-|b|^2+|a-b|^2$ for any functions a and b, we obtain

$$\frac{1}{2k}(|\boldsymbol{u}^{n+1}|^2-|\boldsymbol{u}^{n}|^2+|\boldsymbol{u}^{n+1}-\boldsymbol{u}^{n}|^2)-\nu|\nabla\boldsymbol{u}^{n+1}|^2=\left(\boldsymbol{f}_c^{n+1},\boldsymbol{u}^{n+1}\right)\le\frac{1}{2}|\boldsymbol{u}^{n+1}|^2+\frac{1}{2}\left|\boldsymbol{f}_c^{n+1}\right|^2. \tag{24}$$

If now we add up these inequalities from $n=0$ up to $N-1$ we get

$$|\boldsymbol{u}^{N}|^2-|\boldsymbol{u}^{0}|^2+\sum_{n=0}^{N-1}2\nu k|\nabla\boldsymbol{u}^{n+1}|^2\le\sum_{n=0}^{N-1}k|\boldsymbol{u}^{n+1}|^2+\sum_{n=0}^{N-1}k\left|\boldsymbol{f}_c^{n+1}\right|^2. \tag{25}$$

The discrete Gronwall's inequality now yields (see, e.g., [9])

$$|\boldsymbol{u}^{N}|^2+\sum_{n=0}^{N-1}2\nu k|\nabla\boldsymbol{u}^{n+1}|^2\le|\boldsymbol{u}^{0}|^2+C\sum_{n=0}^{N-1}k\left|\boldsymbol{f}_c^{n+1}\right|^2 \tag{26}$$

which is the discrete version of the classical energy estimate for the Navier–Stokes equations [10]. In this equation and below, C stands for any positive constant, not necessarily the same in its different appearances.

From Eq. (26) we obtain two obvious stability bounds. First, we have that

$$|\boldsymbol{u}^{N}|^2\le|\boldsymbol{u}^{0}|^2+C\sum_{n=0}^{N-1}k\left|\boldsymbol{f}_c^{n+1}\right|^2. \tag{27}$$

This estimate deteriorates as N increases. Nevertheless, it provides a meaningful bound for $|\boldsymbol{u}^{N}|^2$ (and therefore for the kinetic energy of the flow) for the first few time steps, that is, for small T.

The other bound that results from (26) is

$$\sum_{n=0}^{N-1} 2\nu k|\nabla \boldsymbol{u}^{n+1}|^2 \le |\boldsymbol{u}^0|^2 + C\sum_{n=0}^{N-1} k\left|\boldsymbol{f}_c^{n+1}\right|^2. \tag{28}$$

If the kinematic viscosity ν is small, this inequality provides only a poor stability estimate. From the numerical point of view, the norm of the velocity gradient will be out of control.

Up to now, we have not made reference to any particular spatial discretization. Let us assume that this discretization is such that the discrete version of Eq. (28) holds and that $|\nabla\varphi| \ge C|\varphi|/h$ for any discrete function φ, where h is a measure of the size of the discretization (for example, the element diameter if finite elements are employed). If now we use this in Eq. (28) we have that

$$\frac{2\nu}{h^2}\sum_{n=0}^{N-1} k|\boldsymbol{u}^{n+1}|^2 \le C|\boldsymbol{u}^0|^2 + C\sum_{n=0}^{N-1} k\left|\boldsymbol{f}_c^{n+1}\right|^2 \tag{29}$$

where now $\boldsymbol{u}$ must be understood as a discrete velocity. Numerically, this stability estimate is useful if h^2/ν is of the order of a time scale of the problem. If ν is very small, so must h be. This sometimes may be prohibitive from the numerical standpoint. However, in the absence of Coriolis and convective forces, estimates (27) and (28) are enough, since we may define $\bar{\boldsymbol{u}} = \nu\boldsymbol{u}$ and work with $\bar{\boldsymbol{u}}$.

Although the reason for the numerical oscillations that can be found due to the convective and the Coriolis terms are similar and, as we have shown, can be traced back to the fact that both are orthogonal to $\boldsymbol{u}$ in the L^2 inner product, there is an important difference between these two terms. Let us consider the simple equation

$$-\nu\Delta\boldsymbol{u} + 2\boldsymbol{\omega}\times\boldsymbol{u} = \boldsymbol{f} \tag{30}$$

again with the boundary condition $\boldsymbol{u} = \boldsymbol{0}$ on $\partial\Omega$. Multiplying it by $\boldsymbol{u}$ first and then by $2\boldsymbol{\omega}\times\boldsymbol{u}$ and integrating over Ω, we find that

$$\nu|\nabla\boldsymbol{u}| \le |\boldsymbol{f}|, \quad |2\boldsymbol{\omega}\times\boldsymbol{u}| \le |\boldsymbol{f}|, \tag{31}$$

respectively. To obtain the second estimate in (31) we have used that $\nabla\boldsymbol{u} : \nabla(2\boldsymbol{\omega}\times\boldsymbol{u}) = 0$, the colon standing for the double contraction of two second-order tensors. We see thus that it is possible to obtain a stability bound for both the derivatives of $\boldsymbol{u}$ and the Coriolis force. However, for the equation

$$-\nu\Delta\boldsymbol{u} + \boldsymbol{u}\cdot\nabla\boldsymbol{u} = \boldsymbol{f} \tag{32}$$

(or for a linearized form of it), it is impossible to obtain any estimate for the convective term without relying on the value of the viscosity.

The numerical behavior of the finite element solution of Eq. (30) is discussed in Ref. [11], where the finite element solution of the stationary Stokes problem with Coriolis force is studied.

Numerical experiments show that the lack of stability that can be anticipated from the previous discussion, in fact, exists. Oscillations occur when the cell Ekman number, defined

as

$$\mathrm{Ek}_h := \frac{\nu}{\omega h^2} \tag{33}$$

is very small; that is, the Coriolis force dominates the viscous one.

3.2. *Preliminaries*

In order to stabilize the numerical solution when Ek_h is very small, we apply now a technique that generalizes the characteristic Galerkin method presented in the previous section. The idea is to discretize the temporal derivative of the velocity taking into account the variation in time of the rotating basis to which we refer this vector field. This basis will be denoted by

$$\mathcal{B}(t) := \{\boldsymbol{e}_1(t), \boldsymbol{e}_2(t), \boldsymbol{e}_3(t)\}. \tag{34}$$

Let us consider that the original coordinate system $\{x_1, x_2, x_3\}$ is referred to the canonical basis $\mathcal{B}(0)$, whereas for time t the coordinates are $\{y_1(t), y_2(t), y_3(t)\}$. Points in this case are denoted by $\boldsymbol{y}$.

The vectors $\boldsymbol{e}_i(t)$ verify the differential equations

$$\frac{\mathrm{d}\boldsymbol{e}_i}{\mathrm{d}t} = \boldsymbol{\omega} \times \boldsymbol{e}_i, \quad i = 1, 2, 3. \tag{35}$$

If we introduce the matrix $\boldsymbol{A}$, of components $A_{ij} = \varepsilon_{ikj}\omega_k$, with ε being the third-order permutation tensor, Eq. (35) may be rewritten as

$$\frac{\mathrm{d}\boldsymbol{e}_i}{\mathrm{d}t} = \boldsymbol{A}\boldsymbol{e}_i, \quad i = 1, 2, 3. \tag{36}$$

This equation results from the fact that the vectors $\boldsymbol{e}_i(t)$ are obtained from a rotation of the vectors $\boldsymbol{e}_i(0)$ given by

$$\boldsymbol{e}_i(t) = \boldsymbol{T}(t)\boldsymbol{e}_i(0), \quad i = 1, 2, 3, \tag{37}$$

where

$$\boldsymbol{T}(t) := \exp(\boldsymbol{A}t). \tag{38}$$

Observe that, since $\boldsymbol{A}$ is skew-symmetric,

$$\boldsymbol{T}^{\mathrm{t}}(t) = \exp(\boldsymbol{A}^{\mathrm{t}}t) = \exp(-\boldsymbol{A}t) = \boldsymbol{T}^{-1}(t); \tag{39}$$

that is, $\boldsymbol{T}(t)$ is orthogonal. From this and Eq. (37) we have the following equations relating basis vectors and coordinates at different times:

$$\boldsymbol{e}_i(t + t') = \boldsymbol{T}(t')\boldsymbol{e}_i(t) = T_{ji}(t')\boldsymbol{e}_j(t) \quad \forall t, t' \geq 0, \tag{40a}$$

$$\boldsymbol{y}(t) = \boldsymbol{T}^{\mathrm{t}}(t)\boldsymbol{x}. \tag{40b}$$

Let us denote by $\boldsymbol{Y}(\bar{\boldsymbol{x}}, \bar{t}; t)$ the trajectory referred to the basis $\mathcal{B}(t)$ of the particle that at time $\bar{t}$ is located at the position $\bar{\boldsymbol{x}}$ referred to the basis $\mathcal{B}(0)$. Using the notation of the previous section, the vector of position of this particle is

$$\boldsymbol{r}(\bar{\boldsymbol{x}}, \bar{t}; t) = X_i(\bar{\boldsymbol{x}}, \bar{t}; t)\boldsymbol{e}_i(0) = Y_i(\bar{\boldsymbol{x}}, \bar{t}; t)\boldsymbol{e}_i(t). \tag{41}$$

If $\boldsymbol{u}(\boldsymbol{y}, t)$ is the velocity field of the spatial points referred to the basis $\mathcal{B}(t)$, the analogous to problem (4) in the rotating basis is

$$\frac{\mathrm{d}}{\mathrm{d}t} Y_i(\bar{\boldsymbol{x}}, \bar{t}; \bar{t}) = u_i(\boldsymbol{Y}(\bar{\boldsymbol{x}}, \bar{t}; t), t) \tag{42a}$$

$$Y_i(\bar{\boldsymbol{x}}, \bar{t}; \bar{t}) = \bar{y}_i(\bar{t}) = T_{ji}(\bar{t})\bar{x}_j \tag{42b}$$

for $i = 1, 2, 3$. In Eq. (42b) we have used Eq. (40b). To simplify the notation, we shall write $\boldsymbol{Y}(t)$ instead of $\boldsymbol{Y}(\bar{\boldsymbol{x}}, \bar{t}; t)$ in the following.

From Eqs. (36), (41), and (42) it follows that the velocity of the particle considered in Eq. (41) is

$$\boldsymbol{v}(\bar{\boldsymbol{x}}, \bar{t}; t) = \frac{\mathrm{d}}{\mathrm{d}t}\boldsymbol{r}(\bar{\boldsymbol{x}}, \bar{t}; t) = u_i(\boldsymbol{Y}(t), t)\boldsymbol{e}_i(t) + Y_i(t)\boldsymbol{A}\boldsymbol{e}_i(t), \tag{43}$$

and the acceleration term in the complete Navier–Stokes equations may be written as

$$\boldsymbol{a}(t) = \frac{\mathrm{d}}{\mathrm{d}t}[u_i(\boldsymbol{Y}(t), t)\boldsymbol{e}_i(t) + Y_i(t)\boldsymbol{A}\boldsymbol{e}_i(t)]. \tag{44}$$

This expression accounts for the substantial derivative and the Coriolis and centrifugal forces in Eq. (1a) if we particularize it for $t = \bar{t}$.

Another result that we shall need is the expression of the differential operators when we change the reference system. The orthogonality of the matrix $\boldsymbol{T}(t)$ in Eq. (38) implies that both the expressions for the Laplacian and the gradient of a given scalar function φ are independent of the coordinate system used to compute them; that is, we have that

$$\frac{\partial^2}{\partial x_i \partial x_i}\varphi(\boldsymbol{x}) = \frac{\partial^2}{\partial y_i \partial y_i}\varphi(\boldsymbol{T}(t)\boldsymbol{y}), \tag{45a}$$

$$\frac{\partial}{\partial x_i}\varphi(\boldsymbol{x})\boldsymbol{e}_i(0) = \frac{\partial}{\partial y_i}\varphi(\boldsymbol{T}(t)\boldsymbol{y})\boldsymbol{e}_i(t). \tag{45b}$$

All these expressions will be used in the sequel.

3.3. *Time Discretization in the Inertial Basis*

The idea now is to discretize the Navier–Stokes equations, referring all the vectors to the inertial basis. In particular, we consider the vectors of the basis $\mathcal{B}(t)$ referred to the basis $\mathcal{B}(0)$.

Let us obtain first the expression of the momentum equation in the inertial basis but in terms of the coordinates $\{y_1(t), y_2(t), y_3(t)\}$. Starting with the force vector, let us write it as

$$\boldsymbol{f} = f_i^0(\boldsymbol{x}, t)\boldsymbol{e}_i(0) = f_i(\boldsymbol{y}, t)\boldsymbol{e}_i(t), \tag{46}$$

where the components f_i and f_i^0 are related through both a change of basis and a change of coordinates, that is,

$$f_i(\boldsymbol{y}, t) = T_{ji}(t)\, f_j^0(\boldsymbol{x}, t). \tag{47}$$

For the pressure term we have that

$$\frac{\partial}{\partial x_i}\, p(\boldsymbol{x}, t)\boldsymbol{e}_i(0) = \frac{\partial}{\partial y_i}\, p(\boldsymbol{y}, t)\boldsymbol{e}_i(t), \tag{48}$$

where we have made use of Eq. (45b) and we have denoted again by $p(\boldsymbol{y}, t)$ the expression of the pressure in terms of $\boldsymbol{y}$.

If $\boldsymbol{v}(\boldsymbol{x}, t)$ is the velocity field in terms of $\boldsymbol{x}$ and referred to $\mathcal{B}(0)$, using Eqs. (43) and (45a) we get

$$\begin{aligned}\Delta_x \boldsymbol{v}(\boldsymbol{x}, t) &= \Delta_x u_i(\boldsymbol{T}^{\mathrm{t}}(t)\boldsymbol{x}, t)\boldsymbol{e}_i(t) + \Delta_x(T_{ji}x_j)\boldsymbol{A}\boldsymbol{e}_i(t)\\ &= \Delta_y u_i(\boldsymbol{y}, t)\boldsymbol{e}_i(t).\end{aligned} \tag{49}$$

For the sake of clarity, we have used a subscript to indicate the coordinates with respect to which the Laplacian is computed but will be omitted in the following.

From Eqs. (44), (46), (48), and (49) we finally have that the conservation of momentum for a particle of incompressible fluid the trajectory of which is $\boldsymbol{Y}(t)$ leads to the equation

$$\begin{aligned}&\frac{\mathrm{d}}{\mathrm{d}t}[u_i(\boldsymbol{Y}(t), t)\boldsymbol{e}_i(t) + Y_i(t)\boldsymbol{A}\boldsymbol{e}_i(t)] - \nu\Delta\boldsymbol{u}_i(\boldsymbol{Y}(t), t)\boldsymbol{e}_i(t)\\ &\quad + \frac{\partial p}{\partial y_i}(\boldsymbol{Y}(t), t)\boldsymbol{e}_i(t) - f_i(\boldsymbol{Y}(t), t)\boldsymbol{e}_i(t) = \boldsymbol{0}.\end{aligned} \tag{50}$$

This equation may be considered written in the *inertial* basis $\mathcal{B}(0)$, provided that the vectors $\boldsymbol{e}_i(t)$ are expressed in this basis. The basic idea of the method proposed in this paper is to discretize now this equation, taking into account the fact that the vectors $\boldsymbol{e}_i(t)$ depend on time. Using the Crank–Nicolson scheme as in the previous section to perform the time discretization yields

$$\begin{aligned}&\frac{1}{k}[u_i(\boldsymbol{Y}(t_{n+1}), t_{n+1})\boldsymbol{e}_i(t_{n+1}) + Y_i(t_{n+1})\boldsymbol{A}\boldsymbol{e}_i(t_{n+1}) - u_i(\boldsymbol{Y}(t_n), t_n)\boldsymbol{e}_i(t_n) - Y_i(t_n)\boldsymbol{A}\boldsymbol{e}_i(t_n)]\\ &\quad - \frac{\nu}{2}[\Delta\boldsymbol{u}_i(\boldsymbol{Y}(t_{n+1}), t_{n+1})\boldsymbol{e}_i(t_{n+1}) + \Delta\boldsymbol{u}_i(\boldsymbol{Y}(t_n), t_n)\boldsymbol{e}_i(t_n)]\\ &\quad + \frac{1}{2}\left[\frac{\partial p}{\partial y_i}(\boldsymbol{Y}(t_{n+1}), t_{n+1})\boldsymbol{e}_i(t_{n+1}) + \frac{\partial p}{\partial y_i}(\boldsymbol{Y}(t_n), t_n)\boldsymbol{e}_i(t_n)\right]\\ &\quad - \frac{1}{2}[f_i(\boldsymbol{Y}(t_{n+1}), t_{n+1})\boldsymbol{e}_i(t_{n+1}) + f_i(\boldsymbol{Y}(t_n), t_n)\boldsymbol{e}_i(t_n)] = \boldsymbol{0}.\end{aligned} \tag{51}$$

The objective now is to express both the vectors of position $\boldsymbol{Y}(t_{n+1})$ and $\boldsymbol{Y}(t_n)$ and the vectors $\boldsymbol{e}_i(t_{n+1})$ and $\boldsymbol{e}_i(t_n)$ in terms of a reference position $\boldsymbol{Y}(\bar{t})$ and a reference system of vectors $\bar{\boldsymbol{e}}_i := \boldsymbol{e}_i(\bar{t})$. The first part is completely analogous to what was done in the previous section. We shall simply write $\boldsymbol{y}$ for $\boldsymbol{Y}(\bar{t})$, since this position is arbitrary. Also, we

take $\bar{t} = t_n + \gamma k$, where γ is a free parameter. To express $\boldsymbol{e}_i(t_{n+1})$ and $\boldsymbol{e}_i(t_n)$ in terms of $\bar{\boldsymbol{e}}_i$ $(i = 1, 2, 3)$ we shall use the Taylor expansion

$$\begin{aligned}\boldsymbol{e}_i(t_{n+1}) &= \boldsymbol{T}((1-\gamma)k)\bar{\boldsymbol{e}}_i \\ &= \exp[\boldsymbol{A}(1-\gamma)k]\bar{\boldsymbol{e}}_i \\ &= \bar{\boldsymbol{e}}_i + (1-\gamma)k\boldsymbol{A}\bar{\boldsymbol{e}}_i + \frac{1}{2}(1-\gamma)^2k^2\boldsymbol{A}^2\bar{\boldsymbol{e}}_i + O(k^3) \qquad (52a)\end{aligned}$$

and, similarly,

$$\boldsymbol{e}_i(t_n) = \bar{\boldsymbol{e}}_i - \gamma k\boldsymbol{A}\bar{\boldsymbol{e}}_i + \frac{1}{2}\gamma^2k^2\boldsymbol{A}^2\bar{\boldsymbol{e}}_i + O(k^3). \qquad (52b)$$

From problem (42) it is clear that all the approximations along the characteristics found in the previous section can be used here. In particular, using Eqs. (10) and Eqs. (52) it is easy to see that for any vector field $\boldsymbol{w}(\boldsymbol{y}, t) = w_i(\boldsymbol{y}, t)\boldsymbol{e}_i(t)$ we have that

$$\begin{aligned}w_i(\boldsymbol{Y}(t_{n+1}), t_{n+1})\boldsymbol{e}_i(t_{n+1}) &= w_i^{n+1}\bar{\boldsymbol{e}}_i + (1-\gamma)ku_j^n\frac{\partial w_i^n}{\partial y_j}\bar{\boldsymbol{e}}_i \\ &\quad + (1-\gamma)kw_i^n\boldsymbol{A}\bar{\boldsymbol{e}}_i + O(k^2), \qquad (53a)\\ w_i(\boldsymbol{Y}(t_n), t_n)\boldsymbol{e}_i(t_n) &= w_i^n\bar{\boldsymbol{e}}_i - \gamma ku_j^n\frac{\partial w_i^n}{\partial y_j}\bar{\boldsymbol{e}}_i - \gamma kw_i^n\boldsymbol{A}\bar{\boldsymbol{e}}_i + O(k^2), \qquad (53b)\end{aligned}$$

from where it follows that

$$\begin{aligned}&\frac{1}{2}[w_i(\boldsymbol{Y}(t_{n+1}), t_{n+1})\boldsymbol{e}_i(t_{n+1}) + w_i(\boldsymbol{Y}(t_n), t_n)\boldsymbol{e}_i(t_n)] \\ &\quad = w_i^{n+1/2}\bar{\boldsymbol{e}}_i + (1-2\gamma)\frac{k}{2}u_j^n\frac{\partial w_i^n}{\partial y_j}\bar{\boldsymbol{e}}_i + (1-2\gamma)\frac{k}{2}w_i^n\boldsymbol{A}\bar{\boldsymbol{e}}_i + O(k^2). \qquad (54)\end{aligned}$$

Let us concentrate now on the term coming from the discretization of the temporal derivative in Eq. (51) that we split as $\mathcal{T} = \mathcal{T}_1 + \mathcal{T}_2$, where

$$\mathcal{T}_1 = \frac{1}{k}[u_i(\boldsymbol{Y}(t_{n+1}), t_{n+1})\boldsymbol{e}_i(t_{n+1}) - u_i(\boldsymbol{Y}(t_n), t_n)\boldsymbol{e}_i(t_n)], \qquad (55a)$$

$$\mathcal{T}_2 = \frac{1}{k}[Y_i(t_{n+1})\boldsymbol{A}\boldsymbol{e}_i(t_{n+1}) - Y_i(t_n)\boldsymbol{A}\boldsymbol{e}_i(t_n)]. \qquad (55b)$$

Making use of Eqs. (12), (13), and (52) it is found that

$$\begin{aligned}\mathcal{T}_1 &= \frac{1}{k}\left[u_i^{n+1} - u_i^n\right]\bar{\boldsymbol{e}}_i + u_j^{n+1/2}\frac{\partial}{\partial y_j}u_i^{n+1-\gamma}\bar{\boldsymbol{e}}_i + u_i^{n+1-\gamma}\boldsymbol{A}\bar{\boldsymbol{e}}_i \\ &\quad + \frac{1}{2}(1-2\gamma)k\left[u_l^n\frac{\partial}{\partial y_l}\left(u_j^n\frac{\partial}{\partial y_j}u_i^n\right)\bar{\boldsymbol{e}}_i + 2u_l^n\frac{\partial}{\partial y_l}u_i^n\boldsymbol{A}\bar{\boldsymbol{e}}_i + u_i^n\boldsymbol{A}^2\bar{\boldsymbol{e}}_i\right] + O(k^2), \qquad (56a)\\ \mathcal{T}_2 &= u_i^{n+1/2}\boldsymbol{A}\bar{\boldsymbol{e}}_i + y_i\boldsymbol{A}^2\bar{\boldsymbol{e}}_i \\ &\quad + \frac{1}{2}(1-2\gamma)k\left[u_j^n\frac{\partial}{\partial y_j}u_i^n\boldsymbol{A}\bar{\boldsymbol{e}}_i + 2u_i^n\boldsymbol{A}^2\bar{\boldsymbol{e}}_i + y_i\boldsymbol{A}^3\bar{\boldsymbol{e}}_i\right] + O(k^2). \qquad (56b)\end{aligned}$$

If now we use the identity

$$u_i^n \boldsymbol{A}^2 \bar{\boldsymbol{e}}_i = u_l^n \frac{\partial}{\partial y_l} y_i \boldsymbol{A}^2 \bar{\boldsymbol{e}}_i, \tag{57}$$

the temporal term $\mathcal{T} = \mathcal{T}_1 + \mathcal{T}_2$ can be written as

$$\begin{aligned}\mathcal{T} = {} & \frac{1}{k}\left[u_i^{n+1} - u_i^n\right]\bar{\boldsymbol{e}}_i + u_j^{n+1/2}\frac{\partial}{\partial y_j}u_i^{n+1-\gamma}\bar{\boldsymbol{e}}_i + \left(u_i^{n+1-\gamma} + u_i^{n+1/2}\right)\boldsymbol{A}\bar{\boldsymbol{e}}_i + y_i\boldsymbol{A}^2\bar{\boldsymbol{e}}_i \\ & + \frac{1}{2}(1-2\gamma)ku_l^n\frac{\partial}{\partial y_l}\left[u_j^n\frac{\partial}{\partial y_j}u_i^n\bar{\boldsymbol{e}}_i + 2u_i^n\boldsymbol{A}\bar{\boldsymbol{e}}_i + y_i\boldsymbol{A}^2\bar{\boldsymbol{e}}_i\right] \\ & + \frac{1}{2}(1-2\gamma)k\boldsymbol{A}\left[u_j^n\frac{\partial}{\partial y_j}u_i^n\bar{\boldsymbol{e}}_i + 2u_i^n\boldsymbol{A}\bar{\boldsymbol{e}}_i + y_i\boldsymbol{A}^2\bar{\boldsymbol{e}}_i\right] + O(k^2).\end{aligned} \tag{58}$$

The final semidiscrete scheme can be obtained by using this and Eq. (54) in Eq. (51). All the vectors will be expressed in terms their components referred to the basis $\mathcal{B}(\bar{t}) = \{\bar{\boldsymbol{e}}_1, \bar{\boldsymbol{e}}_2, \bar{\boldsymbol{e}}_3\}$. We may therefore write the momentum equations in this basis.

For the incompressibility condition, from Eq. (43) it is easy to see that

$$\nabla_x \cdot \boldsymbol{v}(\boldsymbol{x}, t) := \frac{\partial v_i}{\partial x_i} = \frac{\partial}{\partial x_i}[u_j(\boldsymbol{y}, t)T_{ij}(t) + y_j A_{il}T_{lj}(t)] = \frac{\partial u_i}{\partial y_i}(\boldsymbol{y}, t), \tag{59}$$

which we write simply $\nabla \cdot \boldsymbol{u}$. Using Eq. (20) for the semidiscrete problem we have to impose that $\nabla \cdot \boldsymbol{u}^{n+1} = 0$.

From the results obtained, we see that the final semidiscrete problem to be solved is

$$\begin{aligned}&\frac{1}{k}[\boldsymbol{u}^{n+1} - \boldsymbol{u}^n] + \boldsymbol{u}^{n+1/2}\cdot\nabla\boldsymbol{u}^{n+1-\gamma} + \boldsymbol{\omega}\times(\boldsymbol{u}^{n+1-\gamma} + \boldsymbol{u}^{n+1/2}) - \nu\Delta\boldsymbol{u}^{n+1/2} + \nabla p^{n+1/2} \\ &\quad + \boldsymbol{\omega}\times(\boldsymbol{\omega}\times\boldsymbol{r}) - \boldsymbol{f}^{n+1/2} - (2\gamma-1)\frac{k}{2}\boldsymbol{u}^n\cdot\nabla\mathcal{M}^n - (2\gamma-1)\frac{k}{2}\boldsymbol{\omega}\times\mathcal{M}^n = \boldsymbol{0}, \\ &\qquad\qquad \nabla\cdot\boldsymbol{u}^{n+1} = 0.\end{aligned} \tag{60}$$

We have introduced the *spatial residual* of the Navier–Stokes equations

$$\mathcal{M} := \boldsymbol{u}\cdot\nabla\boldsymbol{u} + 2\boldsymbol{\omega}\times\boldsymbol{u} - \nu\Delta\boldsymbol{u} + \nabla p + \boldsymbol{\omega}\times(\boldsymbol{\omega}\times\boldsymbol{r}) - \boldsymbol{f} \tag{61}$$

and we have denoted again by $\boldsymbol{r}$ the vector of position referred to $\mathcal{B}(\bar{t})$.

In the following section we shall use the finite element method for the space approximation. We shall apply the Galerkin method to problem (60), which has been obtained from a discretization in time in the inertial basis. This is why we call our approach the *inertial Galerkin method*.

As in the previous section for the characteristic Galerkin method, once arrived at problem (60) the terms appearing there may be evaluated at different times leading to different schemes. The important point is the presence of the terms with $\mathcal{M}$ that contribute to enhance the numerical stability of these possible schemes. Also, as it has been pointed out before, other schemes of higher order may be derived using the previous ideas.

To close this section, let us remark that similar arguments can be applied when fractional step methods are employed. Using, for example, the classical approach of Chorin [12] and

Temam [13], the pressure term can be dropped from the time discrete equation (51) and then the resulting velocity projected onto the space of solenoidal vector fields in the classical manner. In any case, the bottom line will be again the appearance of the stabilizing terms in Eqs. (60), with different expressions for the pressure gradient, depending on the type of fractional step method employed. Also, and as it is explained in Ref. [14], the use of some fractional step methods can be interpreted as a purely algebraic operation on the fully discrete system. Of course, this possibility is open using our approach.

4. FINITE ELEMENT APPROXIMATION

4.1. *Weak Formulation*

Problem (60) is a time discrete version of the incompressible Navier–Stokes equations written in a rotating frame of reference. To obtain a fully discrete problem, a spatial discretization must be used. We use here the finite element method.

First, we have to obtain the weak form of problem (60). Let us consider that the boundary conditions are

$$\boldsymbol{u} = \bar{\boldsymbol{u}} \quad \text{on } \Gamma_D, \tag{62a}$$

$$-\nu \frac{\partial \boldsymbol{u}}{\partial n} + \boldsymbol{n}p = \boldsymbol{t} \quad \text{on } \Gamma_N, \tag{62b}$$

where Γ_D and Γ_N are the components of the boundary $\partial\Omega$, where Dirichlet and Neumann types of boundary conditions are prescribed, respectively, and $\bar{\boldsymbol{u}}$ and $\boldsymbol{t}$ are the boundary data. Condition (62b) can be replaced by the prescription of the stress vector on the boundary provided the viscous term in Eq. (1a) is written as the divergence of the strain rate tensor multiplied by the viscosity.

Problem (60) has a free algorithmic parameter γ that defines the reference system (coordinates and basis) at which the equations are discretized. Instead of γ, we can equivalently consider as the algorithmic parameter

$$\tau := (2\gamma - 1)\frac{k}{2}, \tag{63}$$

that we call *intrinsic time*, analogously to the algorithmic parameter found in similar methods, such as SUPG [5].

Let $\boldsymbol{v}$ be a velocity test function (vanishing on Γ_D) and let q be a pressure test function. When the momentum equation in (60) is multiplied by $\boldsymbol{v}$ two new terms appear with respect to the standard Galerkin method. The first of them is

$$-\int_\Omega \boldsymbol{v}\cdot\tau[\boldsymbol{u}^n\cdot\nabla\mathcal{M}^n]\,\mathrm{d}\Omega = -\int_{\partial\Omega}\boldsymbol{n}\cdot\boldsymbol{u}^n\tau\,\boldsymbol{v}\cdot\mathcal{M}^n\,\mathrm{d}\Gamma + \int_\Omega[(\nabla\cdot\boldsymbol{u}^n)\boldsymbol{v}+\boldsymbol{u}^n\cdot\nabla\boldsymbol{v}]\cdot\tau\mathcal{M}^n\,\mathrm{d}\Omega. \tag{64}$$

If we further assume that $\mathcal{M}^n$ vanishes on the boundary $\partial\Omega$ and use the fact that $\boldsymbol{u}^n$ must be divergence-free, we obtain

$$-\int_\Omega \boldsymbol{v}\cdot\tau[\boldsymbol{u}^n\cdot\nabla\mathcal{M}^n]\,\mathrm{d}\Omega = \int_\Omega[\boldsymbol{u}^n\cdot\nabla\boldsymbol{v}]\cdot\tau\mathcal{M}^n\,\mathrm{d}\Omega. \tag{65}$$

When the last term in the momentum equation of (60) is multiplied by $\boldsymbol{v}$ and integrated we get

$$-\int_\Omega \boldsymbol{v}\cdot[\tau\boldsymbol{\omega}\times\mathcal{M}^n]\,\mathrm{d}\Omega=\int_\Omega[\boldsymbol{\omega}\times\boldsymbol{v}]\cdot\tau\mathcal{M}^n\,\mathrm{d}\Omega. \tag{66}$$

From Eqs. (65) and (66) it is seen that the weak form of problem (60) is

$$\begin{aligned}&\int_\Omega \boldsymbol{v}\cdot\left[\frac{\boldsymbol{u}^{n+1}-\boldsymbol{u}^n}{k}+\boldsymbol{u}^{n+1/2}\cdot\nabla\boldsymbol{u}^{n+1-\gamma}+\boldsymbol{\omega}\times(\boldsymbol{u}^{n+1-\gamma}+\boldsymbol{u}^{n+1/2})\right]\mathrm{d}\Omega\\&\quad+\nu\int_\Omega\nabla\boldsymbol{v}:\nabla\boldsymbol{u}^{n+1/2}\,\mathrm{d}\Omega-\int_\Omega p^{n+1/2}\nabla\cdot\boldsymbol{v}\,\mathrm{d}\Omega-\int_\Omega\boldsymbol{v}\cdot[\boldsymbol{f}^{n+1/2}-\boldsymbol{\omega}\times(\boldsymbol{\omega}\times\boldsymbol{r})]\,\mathrm{d}\Omega\\&\quad-\int_{\Gamma_N}\boldsymbol{v}\cdot\boldsymbol{t}\,\mathrm{d}\Gamma+\int_\Omega(\boldsymbol{u}^n\cdot\nabla\boldsymbol{v}+\boldsymbol{\omega}\times\boldsymbol{v})\cdot\tau\mathcal{M}^n\,\mathrm{d}\Omega=0,\\&\qquad\qquad\int_\Omega q\nabla\cdot\boldsymbol{u}^{n+1}\,\mathrm{d}\Omega=0.\end{aligned} \tag{67}$$

These equations must hold for all appropriate test functions $\boldsymbol{v}$ and q.

4.2. *Space Discretization*

Let us consider now a finite element partition $\{\Omega^e\}$, $e=1,\ldots,n_{\mathrm{el}}$, of the computational domain Ω. From it we construct the approximation spaces to the velocity and the pressure made up of functions which are piecewise polynomials, continuous in the case of the velocity. Functions belonging to such discrete spaces are denoted by a subscript h in the following.

The finite element approximation of the weak statement (67) is in principle straightforward. The velocity $\boldsymbol{u}$ and pressure p must be replaced by finite element approximations $\boldsymbol{u}_h$ and p_h and the test functions must be taken in the finite element spaces. We denote these test functions by $\boldsymbol{v}_h$ and q_h. However, the interpretation of the term that involves the integral of $\mathcal{M}^n$ over Ω needs a little attention. Numerically, we have to give sense to this integral, since the viscous term appears in $\mathcal{M}$. Using only continuous approximations (that is, the standard C^0 approach), the Laplacian of the discrete velocities is not square integrable. However, we may interpret the integrals as it is usually done in residual based stabilization methods [5, 6], that is, as

$$\int_{\Omega'}\left(\boldsymbol{u}_h^n\cdot\nabla\boldsymbol{v}_h+\boldsymbol{\omega}\times\boldsymbol{v}_h\right)\cdot\tau\mathcal{M}_h^n\,\mathrm{d}\Omega:=\sum_{e=1}^{n_{\mathrm{el}}}\int_{\Omega^e}\left(\boldsymbol{u}_h^n\cdot\nabla\boldsymbol{v}_h+\boldsymbol{\omega}\times\boldsymbol{v}_h\right)\cdot\tau\mathcal{M}_h^n\,\mathrm{d}\Omega. \tag{68}$$

For smooth functions, $\int_{\Omega'}=\int_\Omega$, so that the consistency of the method is preserved. The terms appearing in this equation are precisely those responsible for the numerical stability of the finite element scheme.

The velocity and pressure finite element interpolations must satisfy the classical Babuška–Brezzi (BB) stability condition (see, e.g., [15]) if no additional pressure stabilization technique is used. One of the possible choices, used in the third example of the following section, is the Q_2/Q_1 element (continuous multiquadratic velocities, continuous multilinear pressures). In the rest of numerical examples we shall use the well-known Q_1/P_0 element (continuous multilinear velocities, piecewise constant pressures), together with a penalty method to eliminate the pressure at the element level (see, e.g., [16]). This element does not

satisfy the BB condition, but provides optimal rates of convergence for the velocity (see [15] for a further discussion about this controversial element). Also, in the first numerical test we shall compare our results with those obtained using the Q_1 interpolation for both the velocity and the pressure with the Galerkin/least-squares (GLS) approach introduced in Ref. [17] and applied to rotating flows in Ref. [11]. In this case, the term $\boldsymbol{u}_h^n \cdot \nabla \boldsymbol{v}_h + \boldsymbol{\omega} \times \boldsymbol{v}_h$ in Eq. (68) has to be replaced by $\boldsymbol{u}_h^n \cdot \nabla \boldsymbol{v}_h + 2\boldsymbol{\omega} \times \boldsymbol{v}_h - \nu \Delta \boldsymbol{v}_h + \nabla q_h$, where q_h is the pressure test function.

It remains to define how to compute the intrinsic time τ. Based on the analysis made in Ref. [8], we compute it as

$$\tau = \left[F_v \frac{\nu}{h^2} + F_c \frac{U}{h} + F_r \omega \right]^{-1}, \tag{69}$$

where F_v, F_c, and F_r are algorithmic factors that determine the importance of the characteristic viscous, convective, and rotation frequencies. For linear elements, we take $F_v = 4$, $F_c = 2$, and $F_r = 1$, whereas for quadratic elements we take $F_v = 40$, $F_c = 4$, and $F_r = 1$. We compute a value of τ for each element, taking U as the mean velocity and h its element diameter.

5. NUMERICAL EXAMPLES

5.1. *Space Convergence Test*

As a first case, we consider a 2D steady-state test with analytical solution to check the behavior in space of the finite element approximation to problem (67). We take Ω as the unit square and the force term so that the solution of problem (1) is $p = 0$ and $\boldsymbol{u}(x, y) = (f(x)g'(y), -f'(x)g(y))$, with $f(x) = x^2(1-x)^2 \exp(7x)$ and $g(y) = y^2(1-y)^2$. This velocity field vanishes on $\partial\Omega$.

As physical properties we have taken $\nu = 0.005$ and $\omega = 1000$. We have used three uniform finite element meshes (meshes 1, 2, and 3) of 10×10, 20×20, and 40×40 Q_1/P_0 elements, so that the element sizes are $h = 0.1$, $h = 0.05$, and $h = 0.025$, respectively. The resulting values of the element Reynolds number are not very high and for this particular example the standard Galerkin approach works in the absence of the Coriolis force. However, when this force exists, the Galerkin method yields completely oscillatory results. These results are shown in Fig. 1, where also the streamlines obtained using the inertial Galerkin method (IGM) are shown. In this case there are no oscillations.

In Fig. 2 we have plotted the convergence of the velocities obtained with the IGM as the mesh is refined, both in the H^1 and the L^2 norms. These results are compared with those obtained using the GLS method. In both cases, convergence is optimal.

Similar results are obtained in the 3D extension of this example that we consider now. The domain is $\Omega = [0, 1] \times [0, 1] \times [0, 0.4]$ and is first discretized using a coarse mesh of $10 \times 10 \times 4$ elements. We take the force term so as to obtain as exact solution $\boldsymbol{u}(x, y, z) = (h(z) f(x) g'(y), -h(z) f'(x) g(y), 0)$, with $f(x)$ and $g(y)$ as before and $h(z) = z(10 - 25z)$. In order to test the numerical method, we have taken different vectors $\boldsymbol{\omega}$, all with the same norm $\omega = 1000$. In all the cases we have obtained good solutions using the IGM.

In Fig. 3 we plot the velocity vectors obtained for $\boldsymbol{\omega}$ parallel to (1, 1, 1), both for the standard Galerkin method and the IGM. The oscillations found using the former are completely removed by the latter.

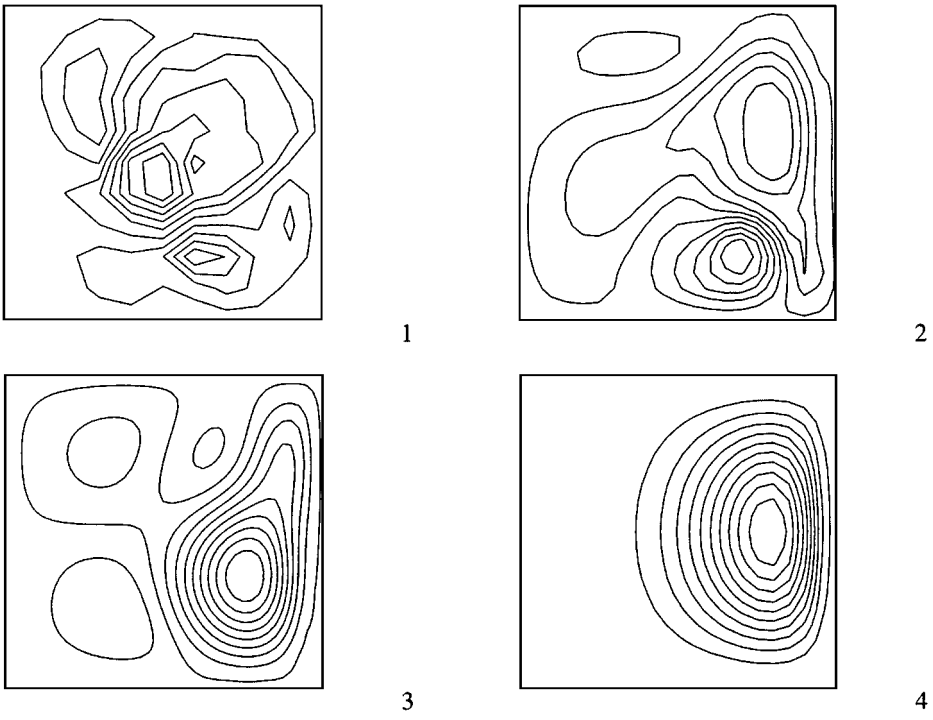

FIG. 1. (1) Streamlines using the Galerkin method with mesh 1; (2) same as (1) with mesh 2; (3) same as (1) with mesh 3; (4) streamlines using the inertial Galerkin method with mesh 1.

5.2. *Ekman Boundary Layers*

This example is intended to illustrate the discussion on the stability of Eq. (30), that is when there are no pressure gradients.

Let us consider a flow over a plane with the no-slip condition that has to match a geostrophic flow $\boldsymbol{u} = (\bar{u}_x, 0, 0)$ as the vertical coordinate z increases. The speed of rotation is assumed to follow the z axis. It is not difficult to see (see, e.g., Ref. [18]) that the solution to this problem is $\boldsymbol{u} = (u_x(z), u_y(z), 0)$, where $u_x(z)$ and $u_y(z)$ are the solution of the equations

$$-\nu \frac{\mathrm{d}^2 u_x}{\mathrm{d}z^2} - 2\omega u_y = 0,$$
$$-\nu \frac{\mathrm{d}^2 u_y}{\mathrm{d}z^2} + 2\omega u_x = 2\omega \bar{u}_x,$$

with the boundary conditions $u_x = u_y = 0$ for $z = 0$ and $u_x \to \bar{u}_x$, $u_y \to 0$ as $z \to \infty$.

We have solved this problem without the assumption on the expression for the velocity, taking as the computational domain $\Omega = [0, 1] \times [0, 1] \times [0, 10]$ and prescribing the velocity to be the same on the four faces parallel to the z axis and to the analytical solution at $z = 10$. The finite element mesh used is made of $5 \times 5 \times 30$ Q_1/P_0 elements.

In Fig. 4 we plot the profiles of the x and y velocities along the vertical direction. It is seen that in this case the results obtained using the Galerkin method are virtually the same

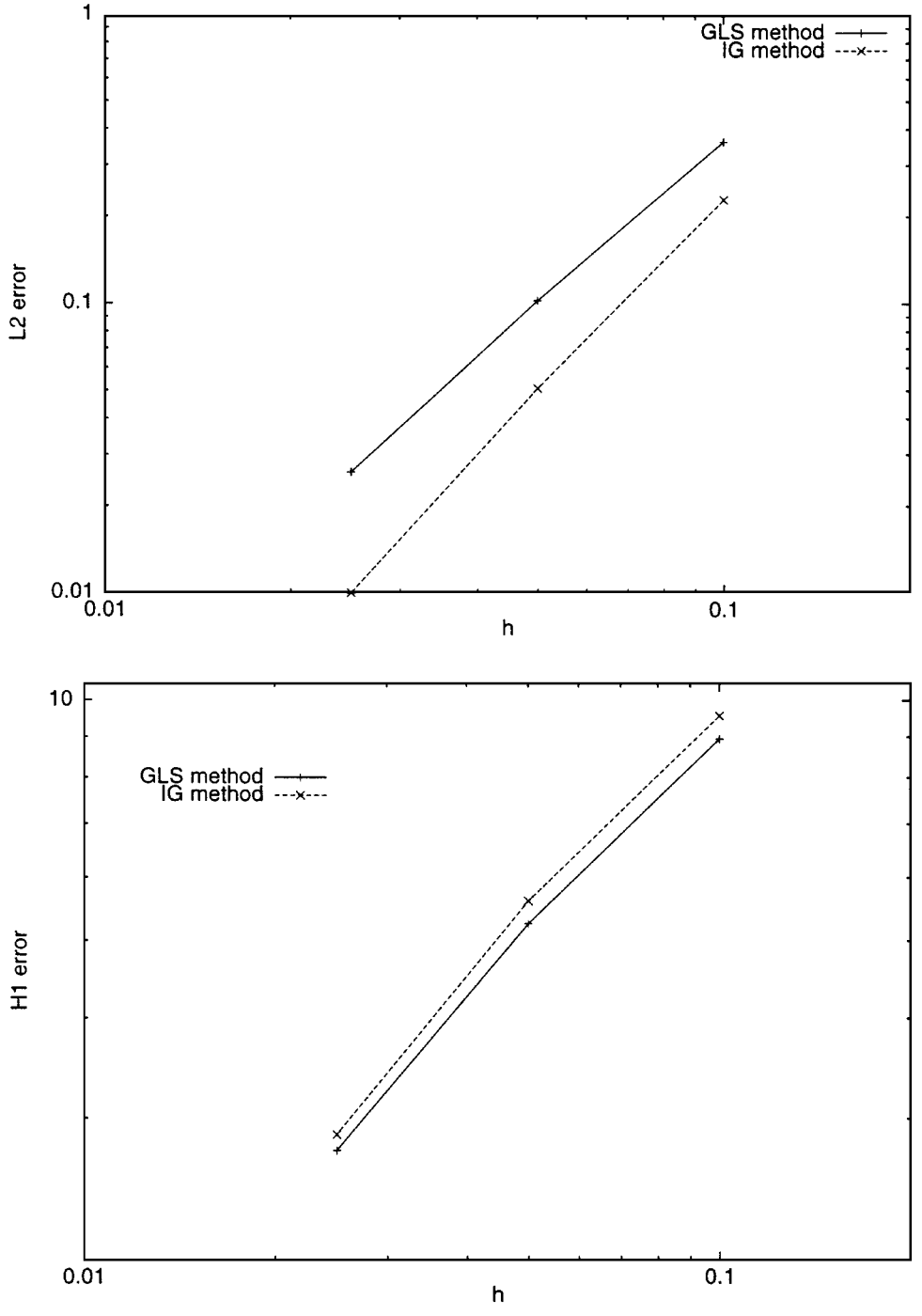

FIG. 2. Convergence of the inertial Galerkin and the GLS methods. Top: L^2 norm; bottom: H^1 norm.

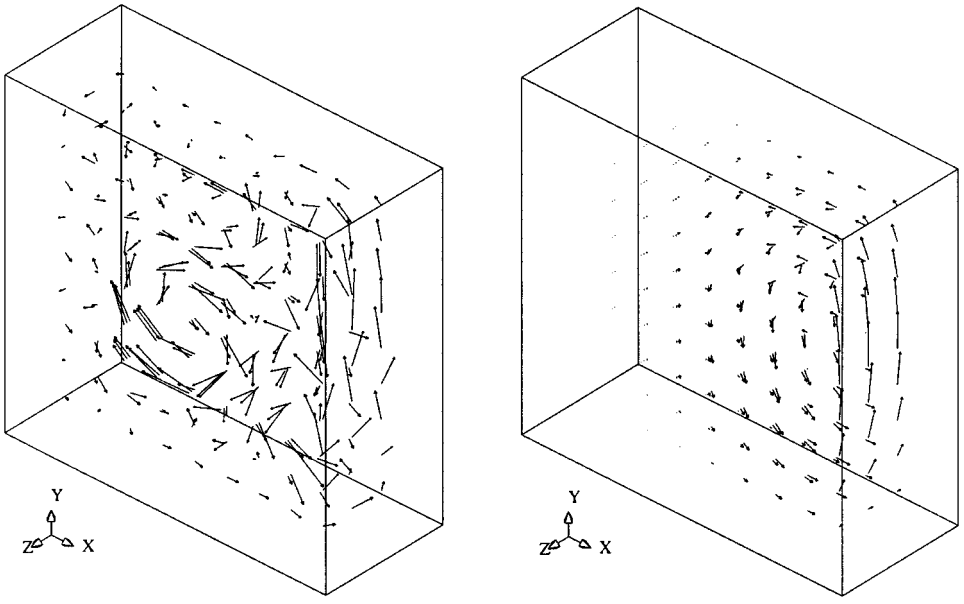

FIG. 3. Velocity vectors for the 3D test case. Left: Galerkin method; right: inertial Galerkin method.

as those obtained using the IG method. For "large" values of the Ekman number ($\nu = 1$) the solution is smooth, but when it decreases ($\nu = 10^{-5}$ in the figure) a boundary layer is created that leads to localized numerical oscillations. This could be expected from Eq. (31), from where its is seen that the L^2 stability is good, but the H^1 is not.

5.3. *Rotating Poiseuille Flow*

In this example we consider a 2D Poiseuille rotating flow. The computational domain is the rectangle $[-2, 2] \times [-1, 1]$ which rotates about the origin with a speed of rotation $\omega = 100$. The Reynolds number is taken small enough so as to neglect the convective term of the Navier–Stokes equations. The problem is therefore linear.

A parabolic velocity profile with maximum velocity (1, 0) is prescribed at the inlet $x = -2$, whereas at the top and bottom walls ($y = -1, 1$) the no-slip condition is employed. If the velocity is also prescribed at the outlet $x = 2$, the velocity solution would not be affected by the fact that the domain rotates (both the Coriolis and centrifugal forces are curl-free, and therefore, they can be written as the gradient of a scalar function that can be included in the pressure). We have used the natural boundary condition (62b) at $x = 2$, with $\boldsymbol{t} = \mathbf{0}$.

Let us consider first the steady-state problem. In turns out that for this very simple problem a velocity "boundary layer" is created at the outlet when the Ekman number decreases. To understand the phenomenon, suppose that the centrifugal force is dropped. The Coriolis force can be replaced by a body force that acts as a traction $\boldsymbol{t}$ at the outlet, pointing downwards at outflow points. This directs the flow towards the bottom of the outlet. This effect is more important the lower the Ekman number is. In order to capture it, we have employed a mesh of 600 Q_2/Q_1 elements (with 2501 nodal points) refined near $y = -1$. The velocity field obtained using this mesh and the Galerkin method with $\nu = 1$ is shown in Fig. 5.

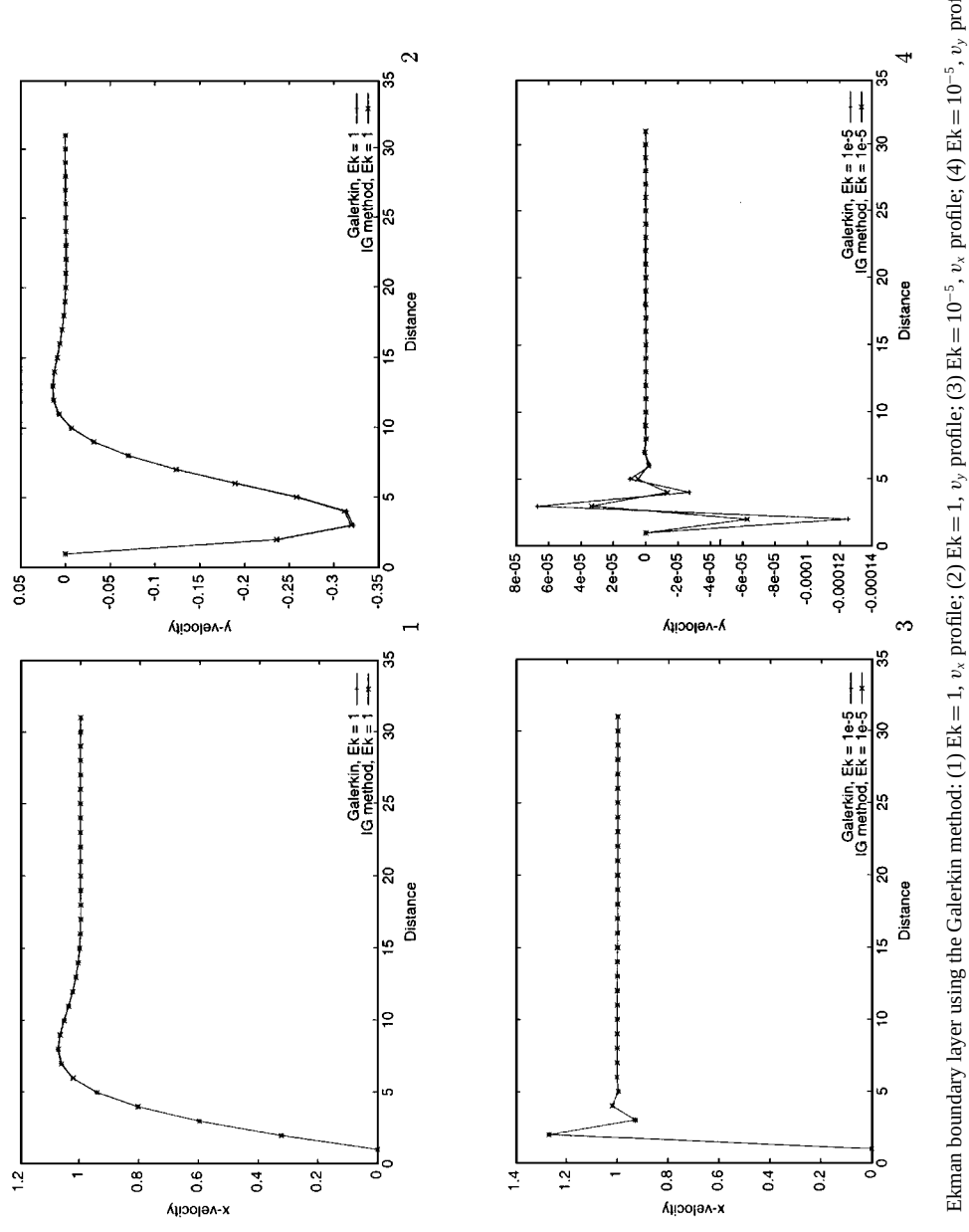

FIG. 4. Ekman boundary layer using the Galerkin method: (1) $\mathrm{Ek} = 1$, v_x profile; (2) $\mathrm{Ek} = 1$, v_y profile; (3) $\mathrm{Ek} = 10^{-5}$, v_x profile; (4) $\mathrm{Ek} = 10^{-5}$, v_y profile.

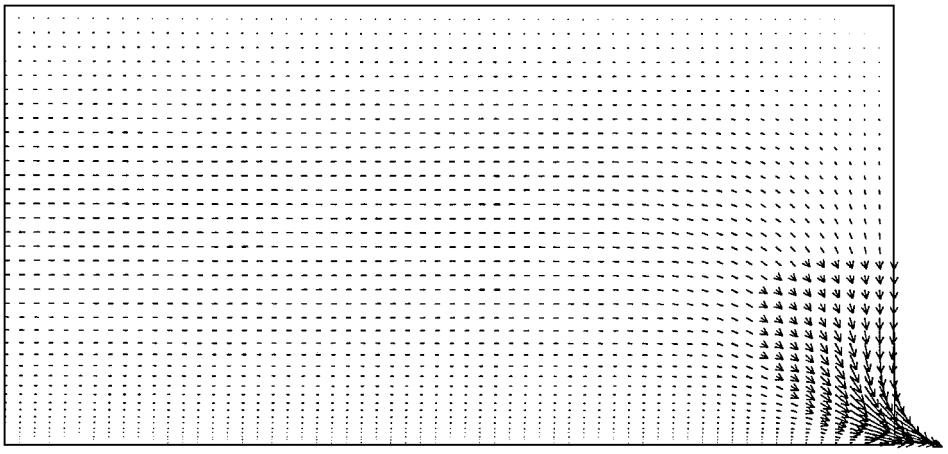

FIG. 5. Velocity field for the steady state rotating Poiseuille flow problem (without centrifugal force). Galerkin method with $\nu = 1$.

The boundary layer created as the Ekman number decreases is shown in Fig. 6. The abscissa is measured in grid spacing units, since otherwise the boundary layer is too thin to be observed. It is seen that the Galerkin method presents global oscillations for $\nu = 10^{-3}$ (that are present in the whole computational domain), whereas the IG method only presents localized boundary layer oscillations. In fact, for smaller values of ν the Galerkin solution is completely oscillatory, whereas the solution obtained with the IG method is perfectly smooth for all ν.

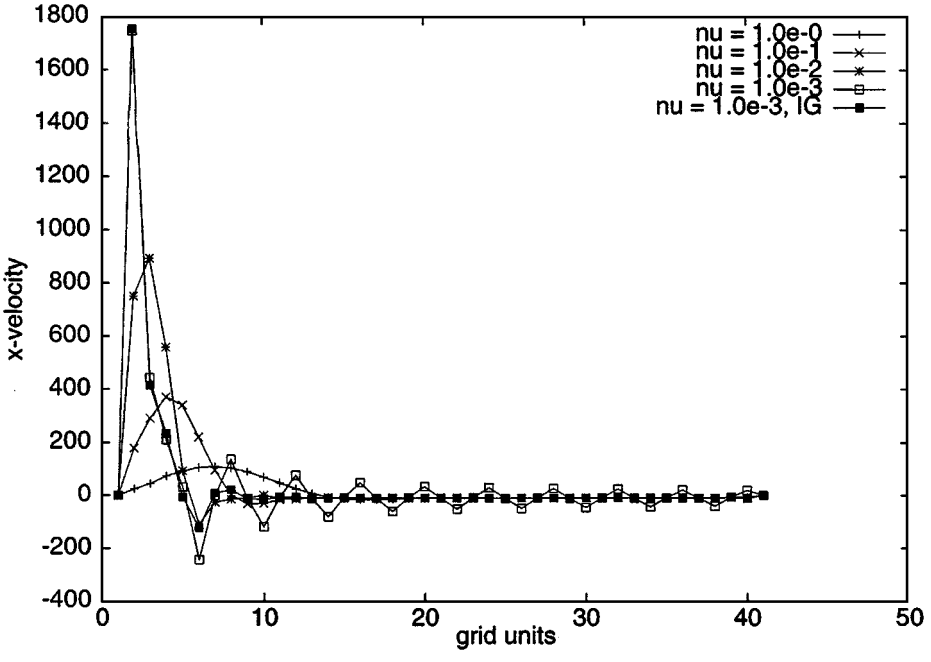

FIG. 6. x-velocity profiles at the outlet for different values of the viscosity using the Galerkin method. Results using the IG method are only shown for $\nu = 10^{-3}$. Abscissa in grid units.

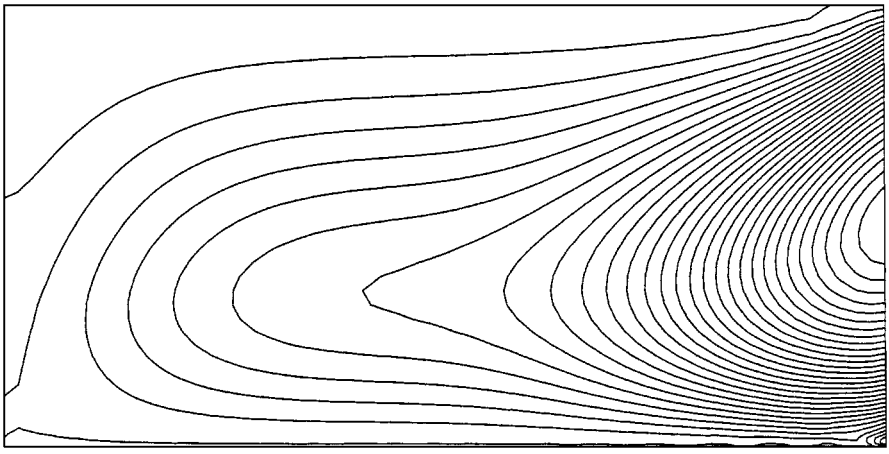

FIG. 7. Streamlines for $\nu = 10^{-3}$ using the IG method for the steady-state problem.

The streamlines computed usign the IG method (incorporating now the centrifugal force) are shown in Fig. 7, whereas the pressure contours are shown in Fig. 8. It is observed that the centrifugal force dominates the pressure and also that the condition $p \approx 0$ at the outlet to which (62b) reduces when ν is very small is well approximated.

Let us turn our attention now to a transient problem. Even though the main reason for the design of the IG method is the problem of the Galerkin approach for the space approximation, it is also interesting to study the approximation properties of the transient scheme (67). For that we have added a rotating body force to the previous scenario that may be thought of as the gravity expressed in the rotating frame. The magnitude of this force is 2000. The results shown correspond to $\nu = 10^{-3}$, the case in which the Galerkin solution has global oscillations.

Figure 9 shows the evolution of the y velocity component in time at the point of coordinates $x = 1.067$, $y = 0.548$ that has been taken as reference. The scheme labelled as "Crank–Nicolson" corresponds precisely to (67), whereas "Euler" corresponds to the scheme obtained by replacing unknowns computed at $t^{n+1/2}$ by unknowns at t^{n+1}. In order

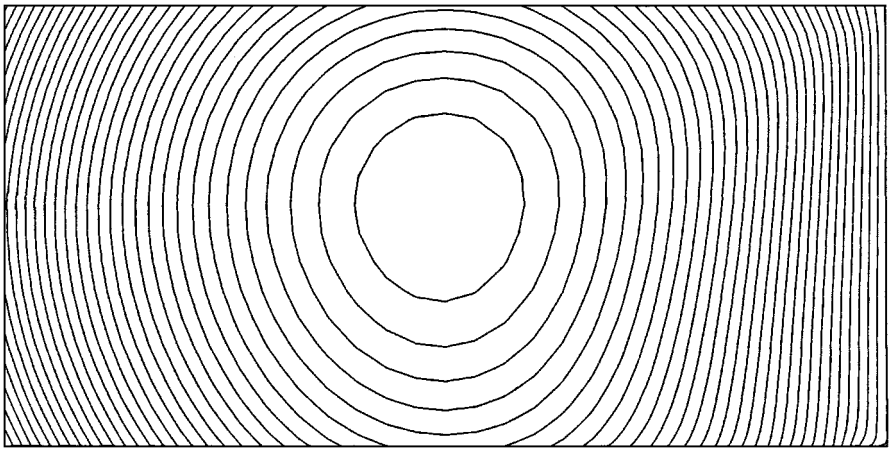

FIG. 8. Pressure contours for $\nu = 10^{-3}$ using the IG method for the steady-state problem.

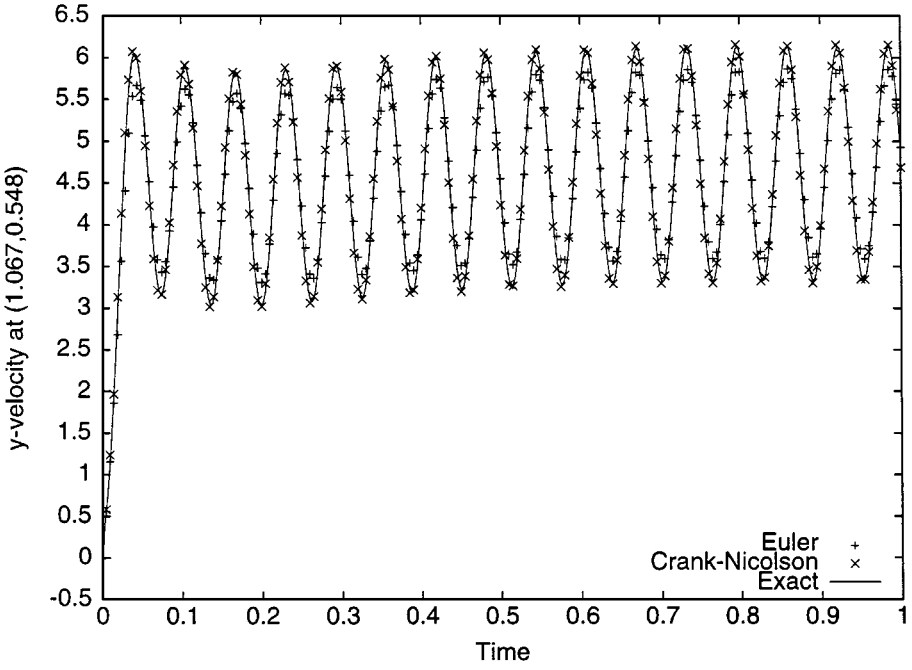

FIG. 9. y-velocity evolution in time at point (1.067, 0.548) using the IG method.

to analyze the accuracy of these schemes, we have solved the problem with a very small time step ($k = 10^{-5}$) and using the Crank–Nicolson scheme. The solution obtained has been used as reference for computing the error plots of Fig. 10. From these, it is seen that for this problem convergence is not optimal. The regression slopes for the x and y velocity errors are 0.80 and 0.64 for the Euler method and 1.23 and 0.67 for the Crank–Nicolson method. This lack of optimality is due to the fact that the solution in this case is not smooth (observe from Eq. (67) that space errors will also affect the time approximation due to the stabilization term). When $\nu = 1$ the optimal rate of convergence is found (2 for the Crank–Nicolson method, 1 for the Euler method), although in this case also the Galerkin method works well (results are not shown).

Finally, in Fig. 11 we plot the streamlines computed using the IG method for $\nu = 10^{-3}$ at two different time steps. It is interesting to remark that the recirculation zone observed at the bottom of the outlet grows and decreases periodically in time, as it can be observed from this figure.

5.4. *Flow Simulation in a Pressure Gear Pump*

In this example we present the numerical simulation of a "real-life" problem using the inertial Galerkin method. The problem consists of the analysis of the steady state oil flow through a tooth of a pressure gear pump, considered as representative of the flow in the whole pump. The technological importance of this example relies on the fact that the numerical simulation allows us to predict the qualitative tendency of a certain pump design to have oil losses, as well as the power needed to make the pump rotate.

We have considered a computational domain discretized using the finite element mesh shown in Fig. 12, which consists of 68,040 Q_1/P_0 elements and 75,936 nodal points. The domain comprises a sector with one tooth. Periodicity boundary conditions are prescribed

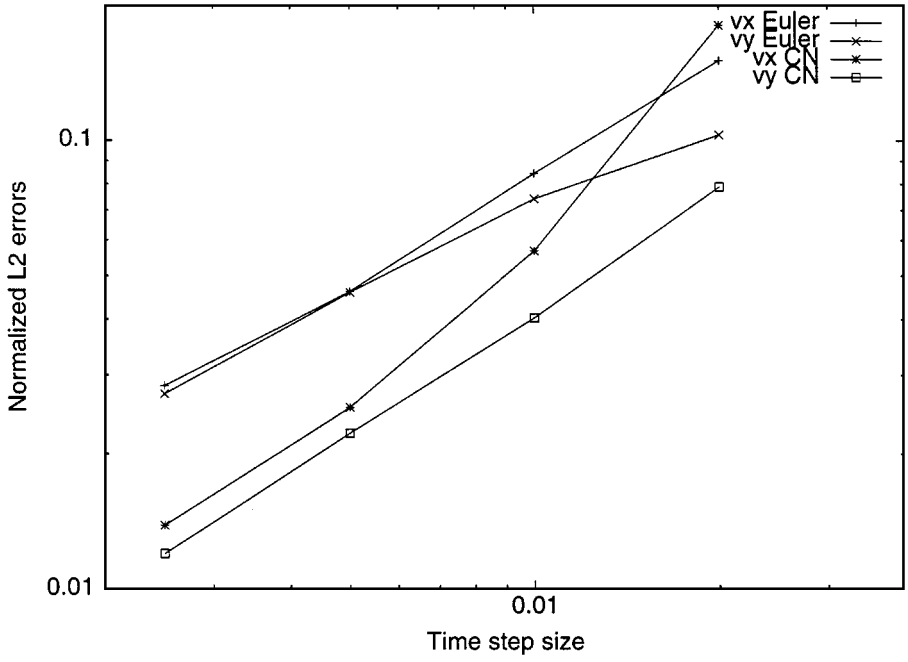

FIG. 10. Discrete L^2 errors in time of the x and y velocity components at point (1.067, 0.548) using the IG method.

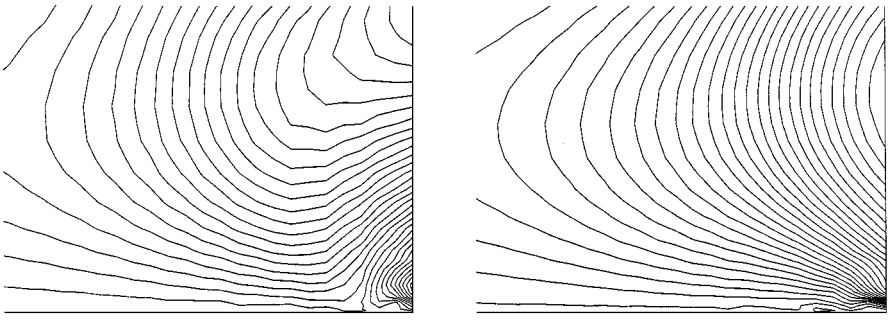

FIG. 11. Streamlines at time step 100 (left) and 120 (right) for $\nu = 10^{-3}$ and $k = 5 \times 10^{-3}$ using the IG method.

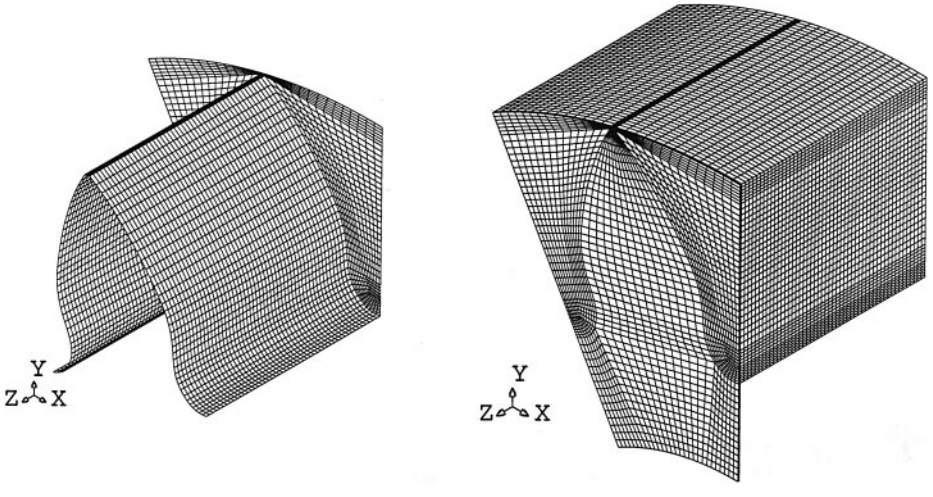

FIG. 12. Finite element mesh on the surface of the tooth (left) and on the surface of the computational domain (right).

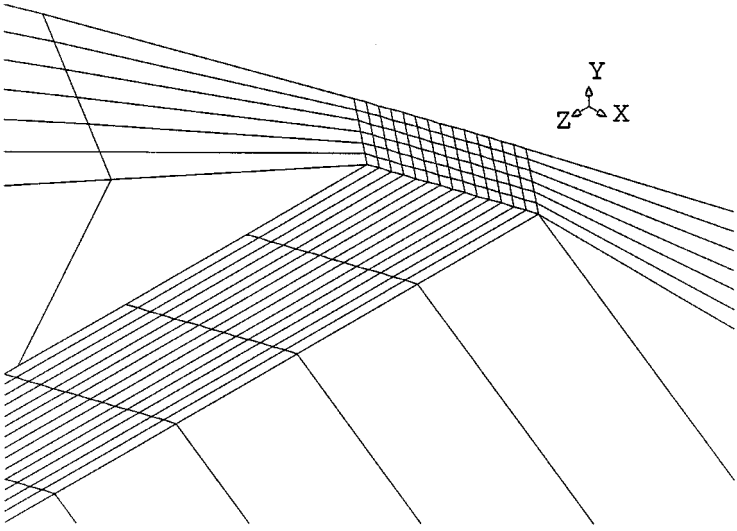

FIG. 13. Detail of the finite element mesh between the tooth and the enclosure.

on the planes limiting the sector. For symmetry reasons, only the domain with one half of the tooth is needed. The velocity is prescribed on the upper enclosure, only 60 μm apart from the tooth (see the detail of the mesh in Fig. 13), to the velocity of rotation ($\omega = 104.72\ \mathrm{s}^{-1}$) times the radius of the pump (18.7 μm). In front of the tooth there is a lateral plate at a distance of 60 mm, where the oil can also flow.

The kinematic viscosity of the oil employed is $\nu = 85.0$ cs. Even though oil flow within pumps is laminar, no attempt has been made in this simulation to capture the boundary layers, and the velocity has been allowed to slip on all the surfaces.

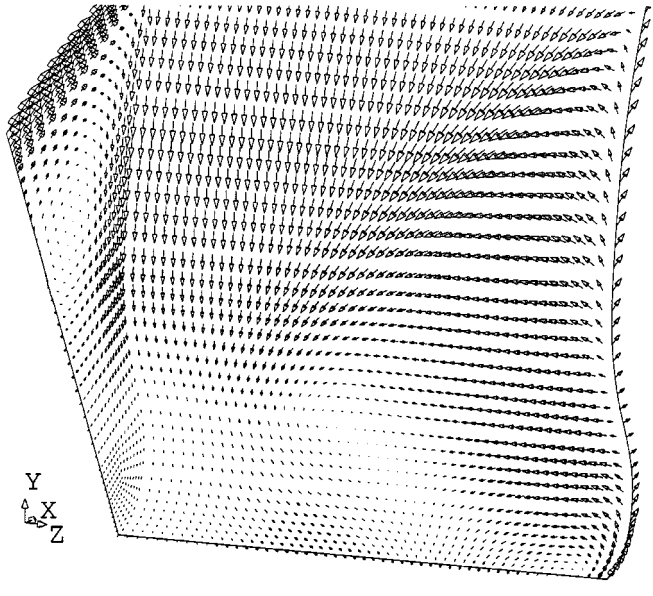

FIG. 14. Velocity field on the left surface of the tooth.

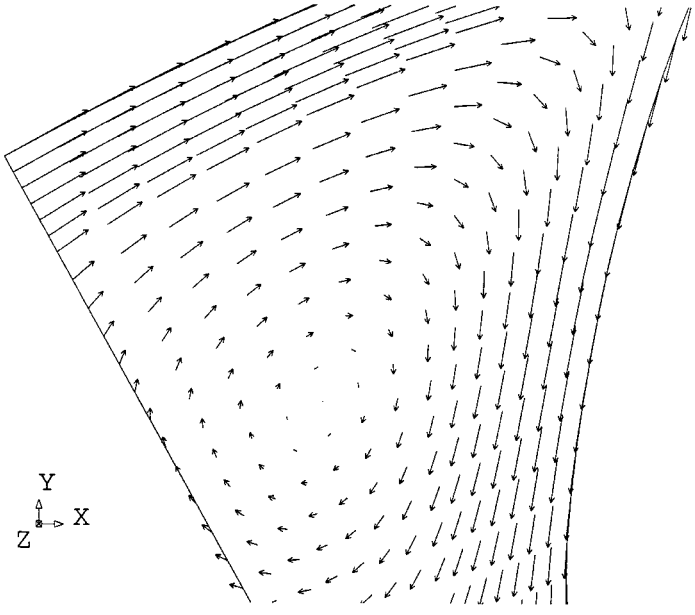

FIG. 15. Vortex in the symmetry plane.

The velocity field computed on the left surface of the tooth is shown in Fig. 14. It is seen that several three-dimensional vortices are formed. A detail of the vortex on the symmetry plane is shown in Fig. 15. Pressure contours on this face are shown in Fig. 16, whereas Figs. 17 and 18 show the velocity field and the pressure contours on the periodicity planes, respectively. The pressure range on these planes is $1.39 \times 10^6\,\mathrm{mm}^2/\mathrm{s}^2$. Finally, Fig. 19 shows the velocity field on the right surface of the tooth.

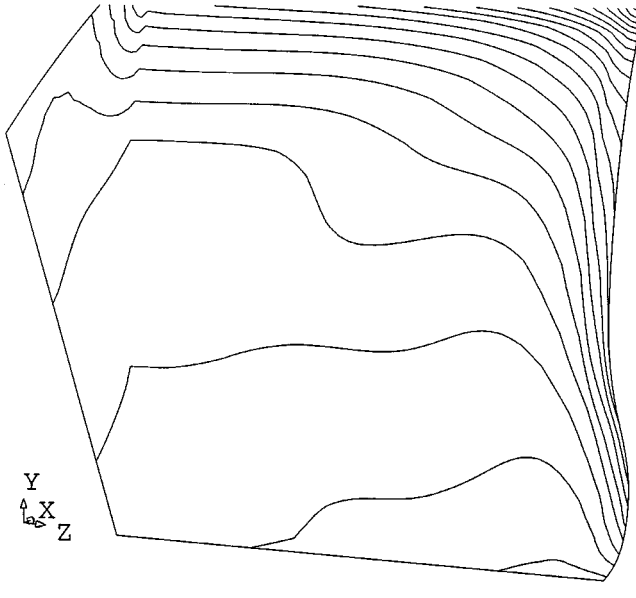

FIG. 16. Pressure contours on the left surface of the tooth.

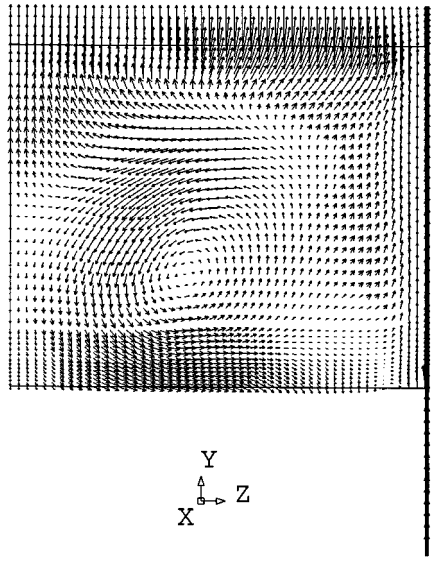

FIG. 17. Velocity field on the periodic walls of the computational domain.

The results of this example are perfectly converged (up to a tolerance of 0.01% in the discrete velocity L^2 norm). Using the standard Galerkin method we have been unable to obtain converged solutions.

6. CONCLUSIONS

In this paper we have presented a stabilization technique to cope with the problems found in the space approximation of the incompressible Navier–Stokes equations when standard centered or Galerkin schemes are used. The method is based on a time discretization of the total time derivative, including the time variation of the basis vectors for rotating flows.

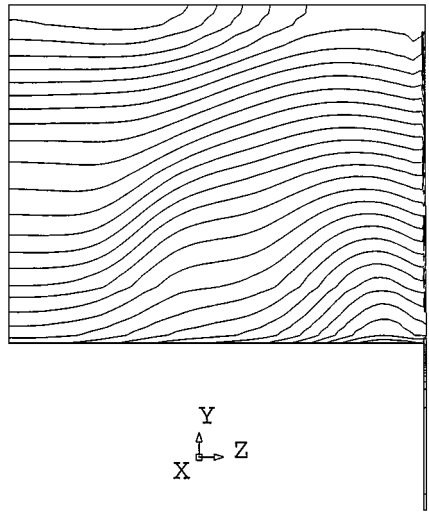

FIG. 18. Pressure contours on the periodic walls of the computational domain.

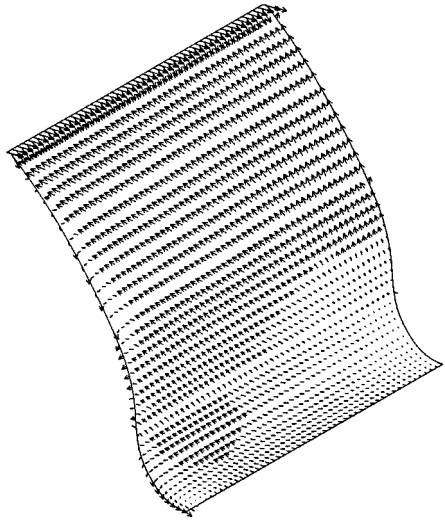

FIG. 19. Velocity field on the right surface of the tooth.

In principle, any time discretization can be used, although we have employed here the generalized trapezoidal rule.

In the absence of Coriolis forces, it has been shown that the classical characteristic Galerkin method is closely related to other methods based on the introduction of streamline diffusion, such as SUPG or Taylor–Galerkin. The basic idea of the derivation is to use a Taylor expansion of the unknowns along the trajectory of the particles. The extension of this idea to rotating flows has led to the introduction of a new term that stabilizes the numerical scheme when the Coriolis force dominates the viscous one. The final numerical method consists in the addition of the stabilizing term given by Eq. (68) to the standard Galerkin formulation of the problem.

It has been shown in a simple test case that the method has an optimal rate of convergence and it has been demonstrated that it is effective to stabilize both convection and rotation. Other numerical examples have also shown the effectiveness of this stabilization technique, even in real flow problems. However, in many real problems it has to be pointed out that the values of the Ekman number for which the Galerkin formulation fails correspond to extremely high values of the Reynolds number. Therefore, in realistic physical situations the problem of important Coriolis force appears, together with complicated flow behavior and, probably, turbulence. Thus, numerical instabilities due to convection are more likely to occur than those due to rotation only.

REFERENCES

1. J. Douglas and T. F. Russell, Numerical methods for convection dominated diffusion problems based on combining the method of characteristics with finite element or finite difference procedures, *SIAM J. Numer. Anal.* **19**, 871 (1982).
2. O. Pironneau, On the transport-diffusion algorithm and its applications to the Navier–Stokes equations, *Numer. Math.* **38**, 309 (1982).
3. R. Löhner, K. Morgan, and O. C. Zienkiewicz, The solution of non-linear hyperbolic equation systems by the finite element method, *Int. J. Num. Meth. Fluids* **4**, 1043 (1984).

4. O. C. Zienkiewicz and R. Codina, A general algorithm for compressible and incompressible flow. Part I. The split, characteristic based scheme, *Int. J. Num. Meth. Fluids* **20**, 869 (1995).
5. A. N. Brooks and T. J. R. Hughes, Streamline upwind/Petrov–Galerkin formulations for convective dominated flows with particular emphasis on the incompressible Navier–Stokes equations, *Comp. Meth. Appl. Mech. Engng.* **32**, 199 (1982).
6. T. J. R. Hughes, L. P. Franca, and G. M. Hulbert, A new finite element formulation for computational fluid dynamics. VIII. The Galerkin/least-squares method for advective-diffusive equations, *Comp. Meth. Appl. Mech. Engng.* **73**, 173 (1989).
7. J. Donea, A Taylor–Galerkin method for convection transport problems, *Int. J. Num. Meth. Engrg.* **20**, 101 (1984).
8. R. Codina, Comparison of some finite element methods for solving the diffusion-convection-reaction equation, *Comp. Meth. Appl. Mech. Engng.* **156**, 185 (1998).
9. J. G. Heywood and R. Rannacher, Finite element approximation of the nonstationary Navier-Stokes problem. II. Stability of solutions and error estimates uniform in time, *SIAM J. Numer. Anal.* **23**, 750 (1986).
10. O. Ladyzhenskaya, *The Mathematical Theory of Viscous Incompressible Flow* (Gordon & Breach, New York, 1963).
11. R. Codina and O. Soto, Finite element solution of the Stokes problem with dominating Coriolis force, *Comp. Meth. Appl. Mech. Engng.* **142**, 215 (1997).
12. A. J. Chorin, Numerical solution of the Navier–Stokes equations, *Math. Comput.* **22**, 745 (1968).
13. R. Temam, Sur l'approximation de la solution des équations de Navier–Stokes par la méthode des pas fractionaires (I), *Arch. Rat. Mech. Anal.* **32**, 135 (1969).
14. J. Blair Perot, An analysis of the fractional step method, *J. Comput. Phys.* **108**, 51 (1993).
15. F. Brezzi and M. Fortin, *Mixed and Hybrid Finite Element Methods* (Springer-Verlag, New York/Berlin, 1991).
16. T. J. R. Hughes, W. K. Liu, and A. Brooks, Finite element analysis of incompressible viscous flows by the penalty function formulation, *J. Comput. Phys.* **30**, 1 (1979).
17. T. J. R. Hughes, L. P. Franca, and M. Balestra, A new finite element formulation for computational fluid dynamics. V. Circumventing the Babuska–Brezzi condition: A stable Petrov–Galerkin formulation for the Stokes problem accommodating equal-order interpolations, *Comput. Meth. Appl. Mech. Engrg.* **59**, 85 (1986).
18. D. J. Tritton, *Physical Fluid Dynamics* (Van Nostrand Reinhold, New York, 1977).